

Benchmarking Gaussian Basis Sets in Quantum-Chemical Calculations of Photoabsorption Spectra of Light Atomic Clusters

Vikram Mahamiya,^{*,†} Pritam Bhattacharyya,^{*,†,‡} and Alok Shukla^{*,†}

[†]*Department of Physics, Indian Institute of Technology Bombay, Powai, Mumbai 400076,
India*

[‡]*Present Address: Institute for Theoretical Solid State Physics, Leibniz IFW Dresden,
Helmholtzstr. 20, 01069 Dresden, Germany*

E-mail: mahamiyavikram@gmail.com; pritambhattacharyya01@gmail.com; shukla@iitb.ac.in

Abstract

The choice of Gaussian basis functions for computing the ground-state properties of molecules, and clusters, employing wave-function-based electron-correlated approaches, is a well-studied subject. However, the same cannot be said when it comes to the excited-state properties of such systems, in general, and optical properties, in particular. The aim of the present study is to understand how the choice of basis functions affects the calculations of linear optical absorption in clusters, qualitatively, and quantitatively. For this purpose, we have calculated linear optical absorption spectra of several small charged and neutral clusters, namely, Li_2 , Li_3 , Li_4 , B_2^+ , B_3^+ , Be_2^+ , and Be_3^+ , using a variety of Gaussian basis sets. The calculations were performed within the frozen-core approximation, and a rigorous account of electron correlation effects in the valence

sector was taken by employing various levels of configuration interaction (CI) approach both for the ground and excited states. Our results on the peak locations in the absorption spectra of Li_3 and Li_4 are in very good agreement with the experiments. Our general recommendation is that for excited-state calculations, it is very important to utilize those basis sets which contain augmented functions. Relatively smaller aug-cc-pVDZ basis sets also yield high-quality results for photoabsorption spectra, and are recommended for such calculations if the computational resources are limited.

Introduction

Gaussian basis functions (GBFs) were initially proposed by Boys for use in computational atomic and molecular quantum mechanics,¹ and over the years have become the preferred basis functions in quantum chemistry.¹ The reason behind the popularity of GBFs is the so-called Gaussian product theorem^{1,2} which allows for analytical results for the expressions of multi-center integrals involving various physical quantities. Nevertheless, one has to be always careful about various convergence related issues when using GBFs, because, unlike Slater basis functions, they do not exhibit correct asymptotic behavior far away from the nuclei. This generally leads to the requirement that a large number of GBFs should be used to achieve convergence, leading to huge memory and CPU-time requirements because the required number of integrals scale as $\approx N^4$, where N is the total number of basis functions. Keeping this in mind, several groups have studied the convergence properties of GBFs over the years, and have come up with schemes to balance accuracy with the computational effort (see, e.g., Refs.^{3,4} for comprehensive reviews). Huzinaga was one of the earliest researchers to optimize GBFs for Hartree-Fock (HF) calculations on atoms.⁵ Ruedenberg and coworkers devised the so-called even-tempered basis set,^{6,7} while Huzinaga and coworkers developed well-tempered basis functions.⁸ Huzinaga and coworkers further developed several contracted basis sets,^{9,10} discussed in detail in Ref.⁴ Pople and coworkers developed a large number of basis sets^{3,4} which enjoy continued popularity even in present

times. One of the most popular minimal basis sets introduced by Pople and coworkers is STO-3G contracted basis set,¹¹ whose purpose was to emulate Slater-type orbitals, using GTFs. Split-valence basis sets are among the most popular extended basis sets introduced by Pople et al.,^{12–15} in which for inner shells contracted minimal basis functions are used, but for the valence shells a split set of basis functions is employed, which consist of both contracted and primitive GTFs. Depending upon the contraction schemes, these basis sets were given names such as 3-21G,¹³ 4-31G,¹² 6-21G,¹⁴ and 6-311G¹⁵, etc. Pople and coworkers also proposed further enlarged basis sets containing polarization and diffuse functions of higher angular momenta, which have since become popular choices in quantum chemistry.^{15–20} Dunning and coworkers introduced a series of extended basis sets, called “correlation-consistent” (CC) basis sets, which are of varying sizes, containing both polarization and diffuse functions.^{21–23} The basic idea behind these CC basis sets is that they recover a significant amount of electron correlation energy in post-Hartree-Fock treatments of corresponding atoms. In addition to the basis sets mentioned here, numerous other sets of basis functions have been developed over the years, for which we refer the reader to review articles by Davidson and Feller,³ and Huzinaga.⁴

Even though so many basis sets have been developed by numerous groups, in most of the reports the criteria for their selection appears to be driven by a good description of the ground state energies of the atoms involved either at the Hartree-Fock level, or in electron-correlated calculations.^{3,4} Previously, Balakina et al.²⁴ have explored the basis set dependence of the linear and non-linear optical properties of conjugated organic molecule p-nitroaniline. They reported that the [4s3p2d/3s] basis set also provides similar results as aug-cc-pVDZ basis set for the calculations of (hyper)polarizability. Parsons et al.²⁵ have explored the basis set dependence of optical rotation calculations of various types of gauges. They found that the origin-invariant length gauge (LG-OI) gauge with aug-cc-pVTZ basis set provides a balance of cost and accuracy for DFT method. Reis and Papadopoulos²⁶ reported that the inclusion of f-functions in the Dunning’s basis sets does not have a large effect on the

electric properties of B4 cluster. Lauderdale and Coolidge²⁷ have explored the effect of basis sets on the non-linear optical properties (hyperpolarizabilities) of linear diacetylenes using time-dependent Hartree-Fock theory. They found that the inclusion of a diffuse ‘d’ function to a standard double-zeta plus polarization basis can significantly improve the frequency-dependent hyperpolarizability. Jabłonski and Palusiak²⁸ have explored the influence of basis sets in Hartree-Fock (HF) and DFT/B3LYP calculations for the values atoms in molecules (AIM) parameters. They found that smaller Dunning’s basis sets, including cc-pVDZ and aug-cc-pVDZ provide poor results as compared to medium-sized Pople-type basis sets. We are not aware of a systematic study in which the basis sets have been examined from the perspective of their performance in excited state calculations. Furthermore, we have also not come across a study which examines the basis sets from the point of view their ability to compute optical properties of atoms and molecules, which involves calculations of transition dipole moments, in addition to excited state energies, and wave functions. In order to fill this void, we decided to undertake a systematic investigation of the influence of basis sets on the qualitative and quantitative description of optical absorption spectra of atomic clusters. In this paper, we have performed calculations of linear optical absorption spectra of several small neutral and cationic clusters, e.g., Li_2 , Li_3 , Li_4 , B_2^+ , B_3^+ , Be_2^+ , and Be_3^+ , using the configuration-interaction (CI) approach. For this purpose, a number of basis sets, namely, 6-311++G(2d,2p), 6-311++G(3df,3pd), cc-pVDZ, cc-pVTZ, aug-cc-pVDZ, and aug-cc-pVTZ, were employed, and their influence on the convergence of excited state energies, wave functions, and transition dipole moments has been systematically examined. In this study, the reason behind our choice of smaller sized atomic clusters and their ions, as against larger ones, is that it is possible to perform highly accurate CI calculations on smaller systems so that the difference between results obtained with different basis sets will be due the nature of basis sets, and not due to the CI approach employed. Based upon our calculations, the main conclusion is that it is very important to include diffuse basis functions in the basis set in order to obtain a good description of the photoabsorption spectra.

Theoretical Approach and Computational Details

General Methodology

All the calculations were performed using the first-principles wave-function-based electron-correlated approaches, using the standard Hamiltonian within the Born-Oppenheimer approximation. The molecular orbitals are expressed in terms of the linear combination of Cartesian-Gaussian type basis functions, also called atomic orbitals (AOs). Although, for such calculations, a number of program packages are available, we employed GAUSSIAN16²⁹ and MELD³⁰ for our calculations. The geometries of all the clusters considered in this work were optimized using GAUSSIAN16 package²⁹ at the coupled-clusters singles-double (CCSD) level of theory, employing a large augmented correlation-consistent polarized valence triple-zeta (aug-cc-pVTZ) basis set.

We perform excited-states calculations for various clusters employing their ground-state optimized geometries, using the configuration-interaction (CI) methodology at various levels of approximation, as implemented in the program package MELD³⁰. The CI calculations yield the vertical excitation energies, the ground and excited state wave functions, and the transition dipole matrix elements connecting the ground and the excited states, which, in turn, are used to compute the optical absorption spectra of various clusters. The level of CI employed in the calculations depends on the size of cluster, the number of valence electrons in cluster, and the number of active orbitals. The linear optical absorption spectra of Li_2 , Li_3 , Li_4 , Be_2^+ , B_2^+ clusters were computed at the full CI (FCI) level, while for Be_3^+ and B_3^+ calculations were performed at the quadruple CI (QCI), and the multi-reference singles-doubles CI (MRSDCI) levels, respectively.

We start the calculations on a given cluster by first performing restricted Hartree-Fock (RHF) calculations on it, and obtain the molecular orbitals (MOs), expressed as linear combinations of the chosen AOs. In order to perform CI calculations, the one- and two-electron Hamiltonian matrix elements are transformed from the AO representation to the MO rep-

resentation. For the FCI calculations, all possible configurations obtained by placing all the valence electrons of the cluster in the given set of MOs, in all possible ways, consistent with the Pauli exclusion principle. In the QCI approach, we first choose a reference configuration, and then generate configurations which are singly-, doubly-, triply-, and quadruply-excited with respect to it. For the ground-state calculations, the reference configuration is normally taken to be the RHF configuration, while for the excited-state calculations one chooses an excited configuration which is closest to the excited state one is trying to calculate. However, both the FCI and the QCI approaches can lead to a very large number of configurations if the number of electrons and the MO basis is large, thus, making the calculations intractable. Therefore, for the larger clusters, we employed the multi-reference singles-doubles configuration-interaction (MRSDCI) approach, as implemented in the MELD package. In this approach, the singly- and doubly-excited configurations are generated from a list of configurations called the reference configurations, chosen by the user. We performed the MRSDCI calculations in an incremental manner, by starting out with a small set of reference configurations that are close to the states (ground or excited) we are targeting. Then we analyze the optical absorption spectra of the cluster calculated from that MRSDCI calculation, and identify a new set of configurations which need to be included in the list of reference configurations based upon their contributions in the wave functions of the targeted states. The procedure is iterated until the calculated optical absorption spectrum converges to within a user-defined threshold. In all the CI calculations, the configurations are actually configuration-state functions (CSFs) which are eigenstates of the point-group symmetry operators, and the total spin operators S^2 and S_z .^{31–42}

The linear optical absorption spectrum of a given cluster is calculated under the electric-dipole approximation, using the formula

$$\sigma(\omega) = 4\pi\alpha \sum_i \frac{\omega_{i0} |\langle i | \hat{\mathbf{e}} \cdot \mathbf{r} | 0 \rangle|^2 \gamma^2}{(\omega_{i0} - \omega)^2 + \gamma^2} \quad (1)$$

Above: (i) $\sigma(\omega)$ represents the optical absorption cross section, (ii) ω is the frequency of incident light, (iii) $\hat{\mathbf{e}}$ denotes the polarization direction of the incident light, (iv) \mathbf{r} is the position operator, (v) α is the fine structure constant, (vi) $\hbar\omega_{i0}$ is the energy difference between ground state (0) and the i^{th} excited state (i), and (vii) γ is the uniform line width associated with each excited state. The line width γ is taken to be 0.1 eV in all our calculations. The sum over index i denotes the sum over all possible excited states. We have restricted this sum in our calculations up to the states corresponding to excitation energies of 10 eV, or less. Additionally, the oscillator strength f_n corresponding to an optical transition from the ground state to the n -th excited state is computed using the standard formula

$$f_n = \frac{2m_e}{3\hbar^2} \Delta E_n \sum_{j=x,y,z} \sum_{\alpha} |\langle n\alpha | O_j | 0 \rangle|^2 \quad (2)$$

above m_e is the electron mass, $|0\rangle$ and $|n\alpha\rangle$ are, respectively the CI wave functions of the ground state and the excited state in question, with α being a degeneracy label, O_j denotes j -th Cartesian component of the electric-dipole operator, while $\Delta E_n = E_n - E_0$ is the excitation energy of the excited state.

Computational Parameters

In this section, we will discuss the convergence of the results with respect two parameters, related to the basis-set-size: (a) number of active orbitals in the CI calculations, and (b) number of CSFs included in the calculations.

Active molecular orbitals

It is well-known that the computational cost at configuration interaction (CI) level of theory increases as N_{act}^6 , where N_{act} is the total number of active molecular orbitals used in the CI calculations. Therefore, the time needed to perform a CI calculation will proliferate rapidly with the increasing values of N_{act} . We have adopted two approaches to reduce the

size of the active MO set: (a) we adopt the frozen-core approximation to eliminate the core orbitals of each atom of the cluster, and (b) for certain cases involving large CI matrices, we delete all those virtual (unoccupied) orbitals from our calculations whose single-particle energies are larger than 1 Hartree. The frozen-core approximation is a standard approach which also has the added advantage of considerably reducing the number of active electrons (n_{elec}) in the calculation. The “1 Hartree cutoff” also doesn’t reduce the accuracy of the calculations because we are interested in low-lying optical excitations below 10 eV, while our cutoff eliminates only those orbitals from the calculations whose energy is larger than 27.21 eV. Both these approximations have been investigated rigorously in our group in earlier calculations.^{36,41–43}

To be specific, in the present set of calculations, we have considered all the virtual orbitals for Li_2 and Be_2^+ clusters, while for Li_3 , Li_4 , Be_3^+ , B_2^+ and B_3^+ clusters we have imposed the 1 Hartree cutoff.

Size of CI expansion

Another important parameter that controls the quality of calculations is the total number of CSFs, N_{total} , included in the CI expansion of the many-particle wave functions of the clusters concerned, both for their ground and the excited states. As mentioned earlier, for a given set of active electrons and MOs, the best possible CI expansion corresponds to the FCI expansion, which becomes intractable for systems with large values of n_{elec} and N_{act} . However, whenever FCI is not possible, we employ one of the restricted CI approaches such as the QCI or the MRSDCI methods. Of the two, it is crucial to examine the convergence of the MRSDCI approach which is based upon singles and doubles excitations from a number of reference configurations (N_{ref}) leading to the final CI expansion with N_{total} CSFs. We examined the convergence of the optical absorption spectrum for the B_3^+ cluster calculated using the MRSDCI method, with respect to N_{ref} , and N_{total} , as presented in Fig. 1.

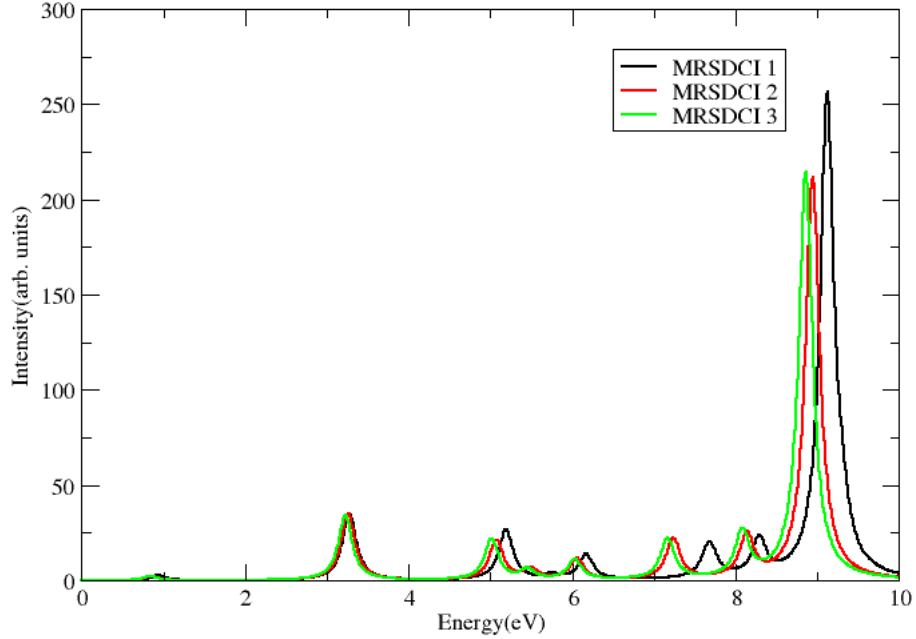


Figure 1: Convergence of the optical absorption spectrum of the B_3^+ computed using the MRSDCI method, with the increasing numbers of reference configurations (N_{ref}). For calculations labeled MRSDCI1, MRSDCI2, and MRSDCI3, values of N_{ref} were 58, 101, and 144, respectively.

In the figure, we plot the absorption spectra of B_3^+ obtained from three MRSDCI calculations of increasing sizes labeled as MRSDCI1, MRSDCI2, and MRSDCI3. In these calculations, the values of parameters N_{ref} and N_{total} were $N_{ref}=58$, $N_{total}=4007873$, $N_{ref}=101$, $N_{total}=5781436$, and $N_{ref}=144$, $N_{total}=8422193$, respectively. From Fig. 1., it is obvious that the spectra obtained using MRSDCI2 and MRSDCI3 calculations are very close to each other, signaling convergence with respect to the size of the MRSDCI expansion.

Results and Discussion

Before discussing the results of our calculations of the optical absorption spectra of various clusters, we first summarize their ground state geometries in Table 1, optimized at the CCSD

level of theory, employing GAUSSIAN16 suite of programs²⁹, and large aug-cc-pVTZ basis sets.

Table 1: The nature of the structure, along with the point group symmetry utilized, during the coupled-cluster singles-doubles (CCSD) geometry optimization calculations are presented below. Additionally, for each cluster, the symmetry of the ground-state wave function, total Hartree-Fock (HF) energy in Hartree (Ha), total CCSD energy (Ha), and the correlation energy (eV) are also presented. During the calculations, aug-cc-pVTZ basis set was employed for each cluster.

Cluster	Structure	Point group	Symmetry of the GS wave function	HF energy (Ha)	CCSD energy (Ha)	Correlation energy (eV)
Li ₂	Linear	D _{2h}	¹ A _g	-14.8715509	-14.9033549	0.87
Li ₃	Linear	D _{2h}	² A _g	-22.3088776	-22.3454346	0.99
Li ₃	Isosceles triangle	C _{2v}	² A ₁	-22.3170594	-22.3557287	1.05
Li ₄	Rhombus	D _{2h}	¹ A _g	-29.7619144	-29.8354840	2.00
Be ₂ ⁺	Linear	D _{2h}	² A _g	-28.9205835	-28.9672583	1.27
Be ₃ ⁺	Linear	D _{2h}	² A _g	-43.5410215	-43.6332325	2.51
B ₂ ⁺	Linear	D _{2h}	² A _g	-48.8344277	-48.9626672	3.49
B ₃ ⁺	Equilateral triangle	D _{3h}	¹ A ₁ '	-73.4445744	-73.7127527	7.27

For each cluster, the table lists the nature of its ground-state structure, point group employed in the calculations, symmetry of the ground state wave function, total energy of the ground state, and the correlation energy. In Table 2, the details related to our CI calculations performed for computing the optical absorption spectra of various clusters are provided. For various clusters, the table lists: (a) the type of CI calculation, (b) the point-group symmetry employed in the calculations, (c) irreducible representations considered for each point group, and (d) for each irreducible representation, the size of the CI expansion (N_{total}) for each cluster are depicted. From Table 2 it is obvious that most of the CI calculations were of the FCI type, which are exact for the chosen set of active MOs. Furthermore, in the calculations in which approaches such as QCI or MRSDCI were used, the size of the CI expansion is quite large. This means that the CI calculations performed in this work are fairly large scale, indicating that the computed optical absorption spectra are numerically accurate. Next, for these clusters, we discuss in detail the calculated ground state geometries, followed by their optical absorption spectra.

Table 2: For each cluster, the type of CI approach used for the calculations of the optical properties, point group symmetry employed during the CI calculations, and the total number of configurations (N_{total}) in the calculation are listed below. The value of N_{total} corresponds to aug-cc-pVTZ basis set based CI calculations.

Cluster	Structure	Method	Point group used	Symmetry	N_{total}
Li ₂	Linear	FCI	C ₁	¹ A	5886
Li ₃	Linear	FCI	C ₁	² A	575960
Li ₃	Isosceles triangle	FCI	C _{2v}	² A ₁ ² B ₁ ² B ₂	137956 129520 137396
Li ₄	Rhombus	FCI	D _{2h}	¹ A _g ¹ B _{1u} ¹ B _{2u} ¹ B _{3u}	1853578 1846246 1844485 1802190
Be ₂ ⁺	Linear	FCI	C ₁	² A	419868
Be ₃ ⁺	Linear	QCI	D _{2h}	² A _g ² B _{1u} ² B _{2u} ² B _{3u}	7393226 7393210 7286869 7286869
B ₂ ⁺	Linear	FCI	D _{2h}	² A _g ² B _{1u} ² B _{2u} ² B _{3u}	6365216 6365216 6323328 6323328
B ₃ ⁺	Equilateral triangle	MRSDCI	C ₁	¹ A	8422193

Geometry

The simplest cluster of lithium is lithium dimer with the $D_{\infty h}$ point group symmetry. We obtained the optimized bond length of Li_2 cluster to be 2.70 Å, as shown in Fig. 2(a). This result is in excellent agreement with the bond length 2.68 Å reported by Wheeler *et al.*⁴⁴, who performed the calculations at the CCSD/CCSD(T) level of theory using the Dunning correlation-consistent polarized core-valence triple/quadruple-zeta cc-pwCVXZ basis sets. Florez *et al.*⁴⁵ performed density functional theory (DFT) calculations using the B3LYP and BLYP functionals, and reported the bond lengths to be 2.70 Å, and 2.71 Å, respectively, again in excellent agreement with our result. Furthermore, our calculated bond length is also in a very good agreement with the experimentally measured value 2.67 Å, reported by Huber⁴⁶.

As far as Li_3 cluster is concerned, two isomers namely linear and isosceles triangle were found to be stable. The equilateral triangular structure of Li_3 cluster is not stable, and undergoes Jahn-Teller distortion to acquire the isosceles triangular structure. The linear structure has the $D_{\infty h}$ point-group symmetry, with the optimized equal bond lengths of 2.90 Å (see Fig. 2(b)), in excellent agreement with the value 2.89 Å, reported by Jones *et al.*⁴⁷. The lowest-energy geometry of the Li_3 cluster is an isosceles triangle with the C_{2v} point-group symmetry. The CCSD-level optimized bond lengths for this structure are found to be 2.68 and 3.07 Å, with the bond angles 51.73° and 64.13° (see Fig. 2(c)). We note that by performing DFT calculations, Jones *et al.*⁴⁷ obtained the bond lengths of 2.82 and 3.37 Å, that are significantly different as compared to our results.

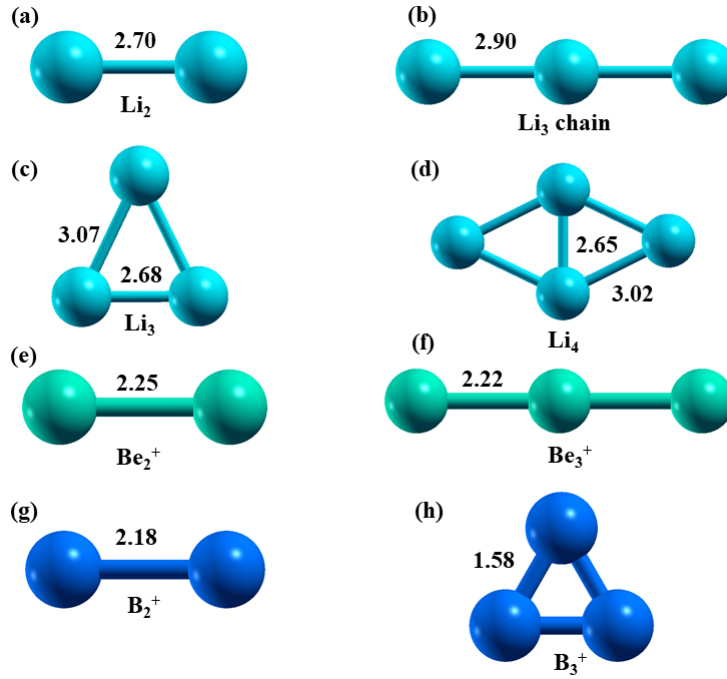


Figure 2: Optimized geometry of (a) Li_2 , (b) Li_3 linear, (c) Li_3 isosceles triangular, (d) Li_4 , (e) Be_2^+ , (f) Be_3^+ linear, (g) B_2^+ , and (h) B_3^+ equilateral triangular clusters considered in this work. The geometry optimization has been performed using the CCSD method, and aug-cc-pVTZ basis sets. All the listed bond lengths are in Å units.

The lowest-energy structure for the Li_4 cluster has a rhombus shape, with D_{2h} point group^{44,47}, as shown in Fig. 2(d). Our optimized bond lengths of the side and minor diagonal of the rhombus structure are 3.02 and 2.65 Å, respectively, which are in excellent agreement with the values 3.04 and 2.62 Å reported by Jones *et al.*⁴⁷.

The optimized bond length of the Be_2^+ cluster with the $D_{\infty h}$ point group is found to be 2.25 Å (see Fig. 2(e)), in good agreement with the reported bond length 2.21 Å, obtained from DFT calculations by Srinivas *et al.*⁴⁸. Our lowest-energy optimized structure of Be_3^+ cluster also has a linear geometry, with two equal bond lengths 2.22 Å, as shown in Fig. 2(f). This value of the bond length is in very good agreement with the value 2.19 Å, computed by Srinivas *et al.*⁴⁸ using DFT.

As far as B_2^+ cluster is concerned, we computed its minimum-energy bond length to be 2.18 Å (see Fig. 2(g)), which is 0.18 Å larger than the value 2 Å reported by Hanley *et al.*⁴⁹.

We attribute this difference to two factors, namely, smaller basis set (6-31G*), coupled with a lower-level CI methodology used by the authors.⁴⁹ Our optimized structure of B_3^+ cluster is an equilateral triangle of sides 1.58 Å, with the D_{3h} point-group symmetry, as shown in Fig. 2(h). Hanley *et al.*⁴⁹ using a CI approach, along with the 6-31G* basis set, also obtained the optimized structure to be an equilateral triangle for the B_3^+ , but with a bond length of 1.53 Å, which is 0.05 Å smaller than our result. We again attribute the differences to the choice of a smaller basis set, coupled with a lower-level correlation methodology as compared to the CCSD approach used by us.

Peak locations

Li_2 dimer, with just two active electrons within the frozen-core approximation, is the smallest many-electron cluster considered in this work. Therefore, very high-quality correlated-electron calculations using large basis sets are possible for this system, not just for its ground states, but also for the excited states. As a result, this case can provide us deep insights into the influence of the choice of basis functions on the calculated excited state properties and the photoabsorption spectra. For the calculations, we employed the frozen-core FCI method using six basis sets of varying sizes, namely, 6-311++G(2d,2p), 6-311++G(3df,3pd), cc-pVDZ, cc-pVTZ, aug-cc-pVDZ and aug-cc-pVTZ, and the computed spectra are presented in Fig. 3(a). All the virtual molecular orbitals generated during the RHF calculations were used in the CI calculations, i.e., no unoccupied orbitals were discarded. As a result, the frozen-core FCI results presented here are the best ones possible for the chosen basis sets.

For the Li_2 dimer, the peak locations in the computed spectra are presented in Table S1 of the Supporting information (SI), from which it is obvious that for the first two peaks the excitation energies calculated using different basis sets are in very good agreement with each other. This is encouraging because from Fig. 3(a) it is obvious that most of the oscillator strength of the absorption spectrum is confined to these two peaks. However, starting from the third peak onward, we start seeing differences in the excitation energies predicted by

different basis sets. For the third peak, the predicted peak locations can be classified in two groups: (a) those predicted by correlation-consistent basis sets cc-pVDZ and cc-pVTZ, and (b) the ones predicted by 6-311G++ and augmented correlation consistent (aug-cc-) class of basis sets. We note that the peak locations predicted by the former class of basis functions have values significantly larger than those predicted by the latter class. Another noteworthy point is that there is very good agreement among the peak locations predicted by the second class of basis sets. As far as the location of the fourth peak is concerned, there is good agreement among the predictions by 6-311++G(3df,3pd) and aug-cc class of basis functions, while the remaining three basis functions predict very different values. The case of the fifth peak is somewhat anomalous in that the agreement among the predictions by any of the basis sets is not good. However, for higher peaks we note that the results from the aug-cc class of basis functions are in good agreement with each other, while other basis functions predict widely differing results. Hong *et al.*⁵⁰ also performed first-principles calculations of the photoabsorption spectra of several Li_n clusters employing the time-dependent density-functional theory (TDDFT) methodology, and for Li_2 their predicted locations of the first two peaks are 1.92 eV and 2.53 eV⁵⁰. On comparing these with our best values of 1.83 eV and 2.57 eV, respectively, we note: (a) our excitation energy for peak I is about 0.09 eV smaller than theirs, while (b) our location for peak II is about 0.04 eV larger than theirs. We attribute these differences to different computational methodologies adopted in the two sets of calculations, and it will be interesting to compare the computational results with the experimental ones, whenever they are available.

The peak locations of the photoabsorption spectra of Li_3 chain are presented in Table S2 of SI, from which it is clear that the locations of the first two peaks converge completely for all the basis sets, similar to the case of dimer. The third peak is the most intense peak of the computed spectra as shown in Fig. 3(b), whose location is in good agreement for all the basis sets except for cc-pVDZ, which predicts higher excitation energy as compared to the rest. From the fourth peak onward, the peak locations can be classified in two similar group

as discussed previously for the case of dimer: the peak locations predicted from correlation-consistent basis sets cc-pVDZ and cc-pVTZ are towards the higher energy side as compared to all other basis sets. It can also be seen that the peak positions corresponding to the two classes of basis sets are in good agreement within the class.

Next, we examine the peak locations in the photoabsorption spectra of Li_3 triangular cluster computed using various basis sets. We note that the peak locations corresponding to the first five peaks are in very good agreement with each other for different basis sets as is obvious from Table S3 of SI. This result is very encouraging because peak IV is the most intense (MI) peak of the computed spectra as presented in Fig. 3(c), and it is crucial for a basis set to be able to accurately describe the MI peaks. The location of this peak is 2.43 eV computed using the aug-cc-pVTZ basis set, which is in a decent agreement with the experimentally detected peak at 2.58 eV by Blanc et al.⁵¹. From the sixth peak onward it was observed that the peak locations calculated using correlation consistent basis sets (cc-pVDZ and cc-pVTZ) do not match with the other classes of basis sets. However, the peak locations computed using the 6-31G class and the aug-cc-pVTZ continue to be in very good agreement with each other till peak VIII, located near 3.8 eV. The locations of higher-energy peaks beyond peak VIII computed using these basis sets are presented in Table S4 for the SI.

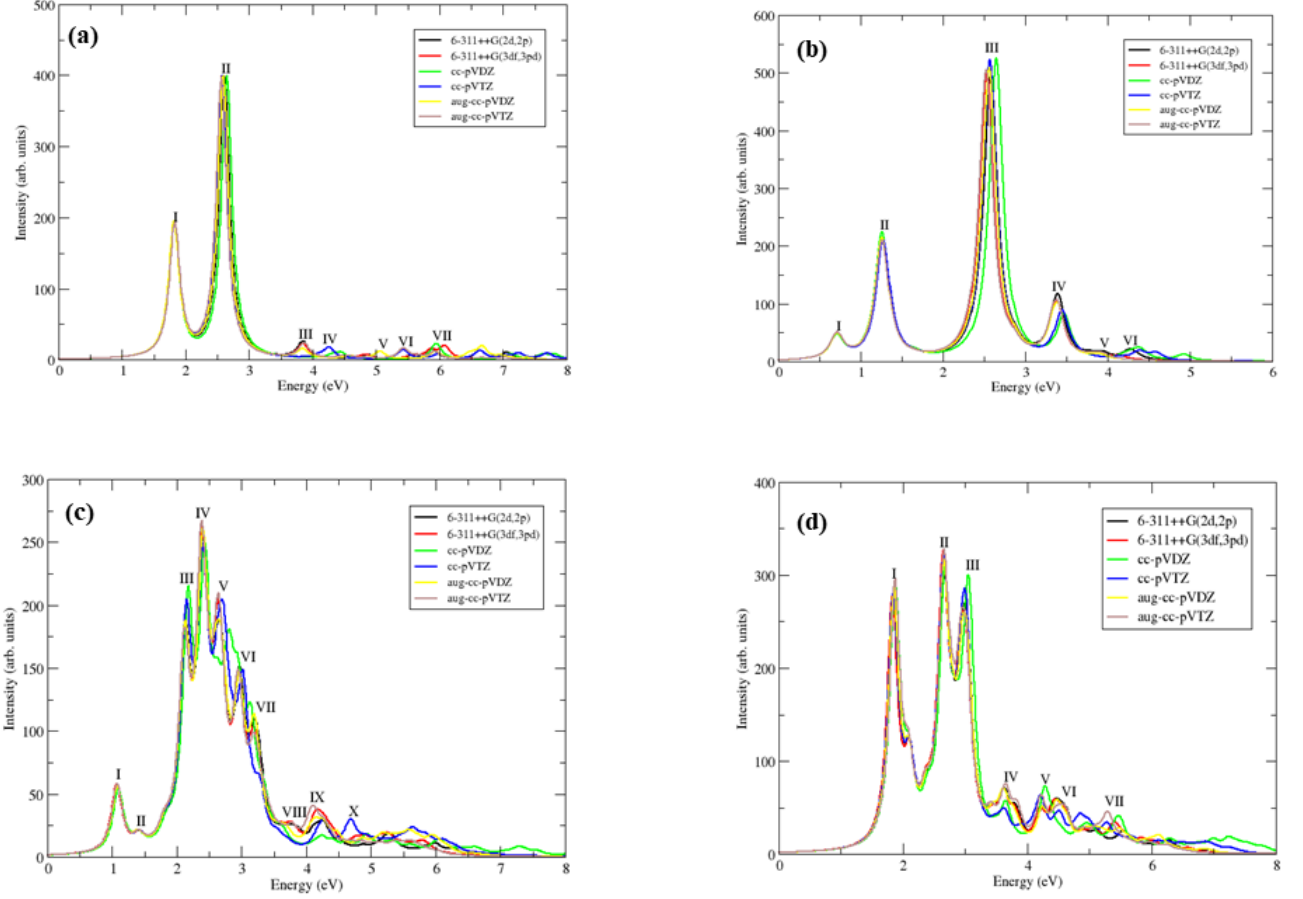


Figure 3: Optical absorption spectra of (a) Li_2 , (b) Li_3 linear, (c) Li_3 triangular, and (d) Li_4 clusters computed using various basis sets and the frozen core FCI method. The uniform line-width 0.1 eV is used to plot the spectrum.

The peak positions of the photoabsorption spectra of Li_4 cluster computed using various basis sets are presented in Table S5 of SI, while the spectra are plotted in Fig. 3(d). We note that for this cluster, the excitation energies of the first five peaks computed using different basis sets are in very good agreement with each other. The first three peaks are much more intense as compared to the higher energy peaks, and in peak III there are slight differences (≈ 0.1 eV) in the peak locations predicted by different basis sets. The two largest basis sets (6-311++G(3df,3pd), and aug-cc-pVTZ) predict the location of peak III at 2.93 eV, while the predictions by the rest of the basis sets are in the range 3.03–3.08 eV. From peak VI

onward we begin to observe differences among the locations predicted by different basis sets, with a tendency towards clustering into different classes. However, the noteworthy point is that the intensity corresponding to these higher energy peaks is very low. As far as the comparison with the experiments is concerned, the first three photoabsorption peaks of the Li_4 cluster located at 1.87 eV, 2.65 eV, and 2.93 eV for aug-cc-pVTZ basis set are in excellent agreement with the experimental measurements of Blanc et al.⁵¹ who detected these peaks at 1.83 eV, 2.65 eV, and 2.93 eV, respectively.

For Be_2^+ cluster, we present the spectra computed by different basis sets in Fig. 4(a), while the corresponding peak locations are presented in Table S6 of SI. We note excellent convergence of the excitation energies up to the sixth peak, beyond which results obtained by different basis sets do not agree much with each other. We further note that Peak V located near 6.30 eV is the most intense peak, and, for that, the predictions of the different basis sets are in a fairly narrow energy range 6.30-6.37 eV.

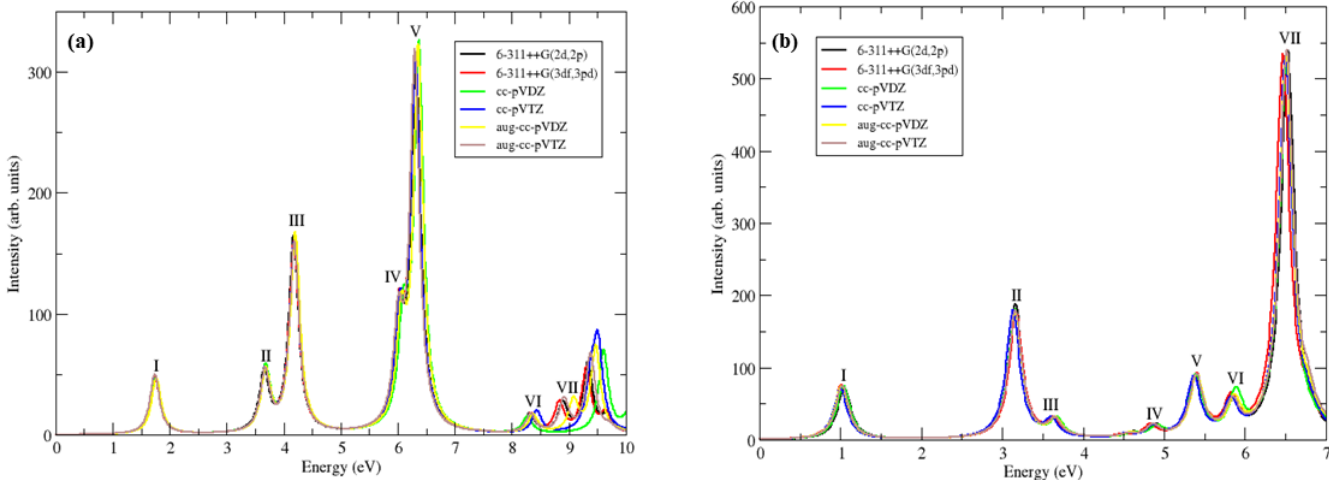


Figure 4: Optical absorption spectra of (a) Be_2^+ and (b) Be_3^+ clusters computed using various basis sets and frozen core FCI and QCI methods, respectively. The uniform line-width of 0.1 eV is used to plot the spectrum.

The excited-states peak locations of Be_3^+ cluster for different basis sets are presented in Table S7 of SI. We notice excellent agreement of the excited-states peak locations up to the

seventh peak which is also the most intense peak of the spectra located near 6.5 eV, as shown in Fig. 4(b). Although the peak location of the sixth peak computed using cc-pVDZ basis set is slightly towards the higher energy region as compared to all other basis sets, but the difference is small. Noteworthy point is that these basis sets are able to achieve convergence in the peak positions in Be_2^+ and Be_3^+ photoabsorption spectra up to much higher excitation energies, as compared to the Li clusters.

The excited-states peak positions corresponding to the photoabsorption spectra of B_2^+ cluster are presented in Table S8 of SI. We notice excellent agreement of the peak energies corresponding to first three peaks for all the basis sets. The fourth peak is the most intense peak of the spectra, as shown in Fig. 5(a) for whose location excellent agreement has been achieved for 6-311++G (2d, 2p), cc-pVTZ, aug-cc-pVDZ, and aug-cc-pVTZ basis sets, indicating complete convergence. However, the excitation energies for peak IV computed using the 6-311++G (3df, 3pd) and cc-pVDZ basis sets are about 0.1 eV higher, as compared to other basis sets. As far as peak V is concerned, which is a very weak shoulder of peak IV, we again observe excellent convergence for all the basis sets, except cc-pVDZ which fails to predict the peak. From the sixth peak onward, as discussed previously, the predicted peak locations can be classified into two groups: (a) larger basis sets of 6-311++G and aug-cc-type, and (b) smaller basis sets cc-pVDZ and cc-pVTZ, with the peak locations predicted by individual classes being in very good agreement with each other.

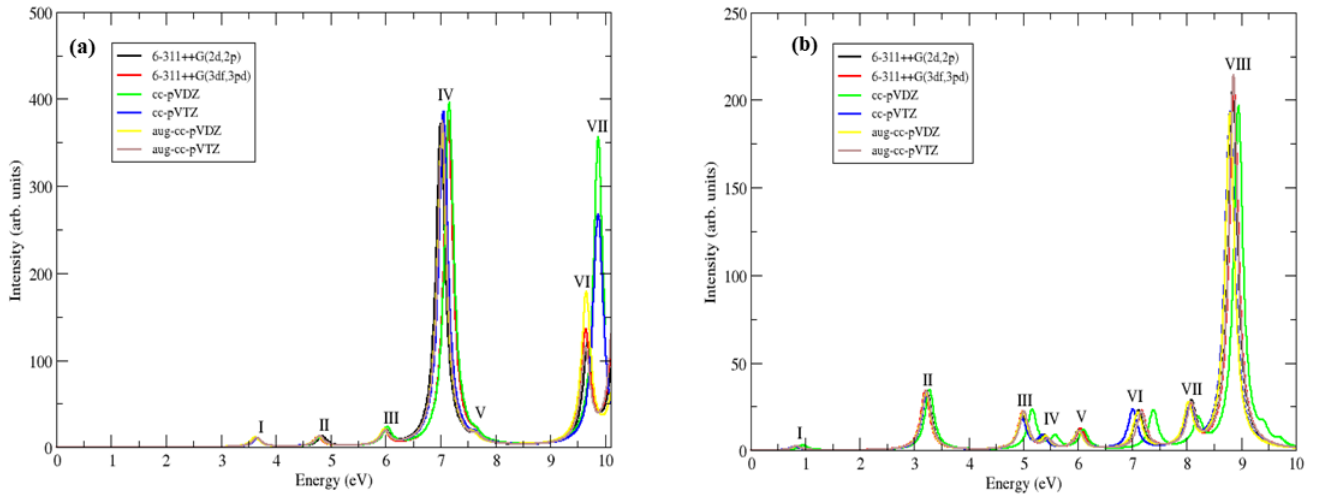


Figure 5: Optical absorption spectra of (a) B_2^+ and (b) B_3^+ cluster computed using various basis sets and frozen core FCI and MRSDCI methods, respectively. The uniform line-width 0.1 eV is used to plot the spectrum.

The peak locations corresponding to the excited-states of the photoabsorption spectra of B_3^+ cluster are presented in Table S9 of SI, while the calculated spectra are plotted in Fig. 5(b). For this cluster, we get eight well-separated peaks in the explored energy range, with peak VIII located near 8.9 eV being the most intense. We note that the peak energies corresponding to all the basis sets converge excellently up to the peak VIII, except those predicted by the cc-pVDZ basis set, which are consistently higher. We have noticed in Fig.4 and Fig.5, only the deep valence excitation energies are dependent on the choice of basis sets. This behavior can be a consequence of the frozen-core approximation, which we have employed in the calculations. To verify this, we have computed the optical absorption spectra of Li_2 and Be_2^+ clusters by also including the core excitations within the large-scale QCI method. We found that the optical spectra of these clusters computed by including core excitations agrees completely with the absorption spectra computed after employing frozen-core approximation, as shown in Fig.S1 and Fig.S2 of the SI. Therefore, the frozen-core approximation does not alter the absorption spectra of small clusters.

Based on the peak positions of the individual clusters discussed above, we observe the

following general trends: (a) peak locations for all the clusters used in this study are in very good agreement for all the basis sets up to the most intense peak of the spectra, except for cc-pVDZ basis set. (b) the excited-states peak locations beyond the most intense peak can be classified in two groups, in which the peak locations calculated using correlation-consistent basis sets do not match with the peak locations computed using all other basis sets, and (c) for the cc-pVDZ basis sets peaks are located at higher energies as compared to the rest of the basis functions. As the basis-set dependence of the optical properties is different for the density functional theory compared to the wave function-based large-scale configuration-interaction method, it will be interesting to explore the optical properties of clusters using time-dependent density functional theory (TD-DFT) and compare it with our results. We found that the first peak of the optical absorption spectra of B_3^+ cluster is located at 0.84 eV when computed using large-scale MRSDCI calculations along with a large aug-cc-pVTZ basis set. However, when the calculations are performed using TD-DFT method with B3LYP functional and the same basis set, it is obtained at 0.95 eV. The most intense peak of the optical absorption spectra is located at 8.85 eV using the MRSDCI approach, which is found to be at 9.35 eV by employing the TD-DFT method. The calculated optical absorption spectra and excited-states peak locations of B_3^+ cluster corresponding to TD-DFT calculations are provided in the Fig.S3 and Table S10 of the SI. We also report that the variations in the peak locations of the photoabsorption spectra of B_3^+ computed using various basis sets and TD-DFT method are lesser than the wave function-based CI method.

Oscillator strength

In addition to the excitation energy, the next important quantity determining the profile of the absorption spectrum is the oscillator strength (f) corresponding to various optical transitions, connecting the ground state to the excited state in question. The oscillator strength calculated using Eq. 2 is determined by the excitation energy of the state involved, and the corresponding transition dipole moment (TDM). The TDM being a matrix element, is, in

turn, determined by the many-particle wave functions of the ground and the excited state that it connects. Another important quantity is the polarization of the photon involved in a given optical transition (peak), which can be measured in oriented samples. The polarization is a consequence of the point-group symmetry of the concerned molecule, and hence should be independent of the basis set employed. In this section, we discuss the convergence of the oscillator strengths and photon polarizations associated with various peaks of the calculated spectra. In Table 3, we present the oscillator strengths corresponding to the first peak, and the most intense peak (peak II) of the spectra of Li_2 computed using different basis functions. Additionally, the table also contains the dominant configurations contributing to the many-particle wave functions of the excited states involved.

Table 3: Comparison of oscillator strengths and the dominant configurations contributing to the many-particle wave functions for peaks I and II of Li_2 cluster calculated using different basis sets. In the ‘‘Polarization’’ column, \parallel indicates photon polarization along the direction of the molecule (longitudinal polarization), while \perp indicates polarization perpendicular to the molecular axis (transverse polarization). Note that the transversely polarized states are doubly degenerate, therefore, the oscillator strength corresponding to those is the sum of both the contributions. ‘H’ and ‘L’ stand for HOMO and LUMO orbitals.

Basis Set	Peak I			Peak II		
	Polarization	f	Configurations	Polarization	f	Configurations
6-311++G(2d,2p)	\parallel	0.460	$ H \rightarrow L\rangle$ $ H \rightarrow L + 3\rangle$	\perp	0.971	$ H \rightarrow L + 2\rangle$ $ H \rightarrow L + 7\rangle$
6-311++G(3df,3pd)	\parallel	0.456	$ H \rightarrow L\rangle$ $ H \rightarrow L + 3\rangle$	\perp	0.966	$ H \rightarrow L + 2\rangle$ $ H \rightarrow L + 7\rangle$
cc-PVDZ	\parallel	0.463	$ H \rightarrow L\rangle$ $ H \rightarrow L; H \rightarrow L + 2\rangle$	\perp	0.970	$ H \rightarrow L + 1\rangle$ $ H \rightarrow L + 1; H \rightarrow L + 5\rangle$
cc-pVTZ	\parallel	0.455	$ H \rightarrow L\rangle$ $ H \rightarrow L + 4\rangle$	\perp	0.969	$ H \rightarrow L + 1\rangle$ $ H \rightarrow L + 6\rangle$
aug-cc-pVDZ	\parallel	0.462	$ H \rightarrow L\rangle$ $ H \rightarrow L + 3\rangle$	\perp	0.972	$ H \rightarrow L + 1\rangle$ $ H \rightarrow L + 6\rangle$
aug-cc-pVTZ	\parallel	0.454	$ H \rightarrow L\rangle$ $ H \rightarrow L + 3\rangle$	\perp	0.966	$ H \rightarrow L + 2\rangle$ $ H \rightarrow L + 7\rangle$

From Table 3 it is obvious that the oscillator strengths computed using various basis functions for both the peaks are in very good agreement with each other. We also note that the direction of the polarization of the photons involved in a given optical transitions are of

the excited-states corresponding to the first and second peak of the spectra of Li_2 cluster are parallel and perpendicular to molecular axis, respectively, irrespective of the basis set.

The oscillator strengths corresponding to the first and most intense peaks of the spectra of Li_3 chain and triangular clusters are presented in Table S11 and Table S12, respectively. We note that the oscillator strengths of the first peaks both of Li_3 chain, and the triangular cluster, computed using the different basis sets are in excellent agreement with each other. The oscillator strengths corresponding to the most intense peaks of Li_3 , i.e. peak III of the chain and peak IV for the triangular cluster, calculated using various basis sets can be classified into two groups: (a) those calculated using correlation-consistent (cc-pVTZ and cc-pVDZ) class of basis sets, and (b) those computed using 6-33++G- and augmented correlation-consistent (aug-cc-) class of basis sets. The oscillator strength calculated by the first class of basis sets is comparatively higher than the second class of basis sets. But, the relative maximum difference between oscillator strengths of different classes is close to 6%, which is fairly acceptable.

The oscillator strengths corresponding to the first and the most intense peak (peak II) in the photoabsorption spectra of Li_4 cluster are presented in Table S13. We note that the oscillator strengths of peak I are in good agreement with each other for all the basis sets except for cc-pVDZ and aug-cc-pVTZ. For these basis sets the oscillator strength is comparatively larger. For peak II, we note that the difference in the oscillator strength computed by cc-pVDZ and 6-311++G (3df, 3pd) basis sets is about 5%, which is again quite small.

We present the oscillator strengths corresponding to the first and the most intense peaks of the cationic beryllium clusters Be_2^+ and Be_3^+ in tables S14, and S15, respectively. We note very good agreement on the oscillator strengths of both the peaks of the Be_2^+ and Be_3^+ clusters for all the basis sets. The maximum relative disagreement we find among the oscillator strengths for a given peak is around 6%.

Finally, we discuss the oscillator strengths of the first and the most intense peaks of the

B_2^+ and B_3^+ clusters presented in tables S16, and S17, respectively. We note that both for B_2^+ and B_3^+ clusters, the oscillator strengths of the first peaks are two orders of magnitude smaller than those of their most intense peaks, indicating that the first peaks for both the clusters are relatively feeble. Nevertheless, the oscillator strengths of the first peaks of the photoabsorption spectra of the two clusters calculated using various basis sets are in very good agreement with each other. As far as the most intense peaks are concerned, both for B_2^+ and B_3^+ we see the following pattern: oscillator strengths computed using 6-311++G- and aug-cc-pVTZ basis sets are in very good agreement with each other, while those computed using other basis sets differ from them somewhat.

Wave function analysis

Next, we examine the dominant configurations contributing to the CI wave functions of the excited states contributing to various peaks. The dominant configurations corresponding to the excited-states CI wave functions of peak I and peak II of Li_2 are presented in Table 3. We note that for peak I, the main contribution to the corresponding excited state wave function is from the singly excited configuration $|H \rightarrow L\rangle$ for all the basis sets. However, the next important configuration to the same wave function depends on the class of basis set employed: (a) it is $|H \rightarrow L+3\rangle$ single excitation when calculations are performed using larger basis sets of the type 6-311++ and aug-cc, but (b) for smaller basis sets, this configuration is found to be $|H \rightarrow L+4\rangle$ for cc-PVTZ basis, and $|H \rightarrow L; H \rightarrow L+2\rangle$ for the cc-PVDZ set. Peak II is due to two degenerate excited states to which the dominant contributions are from configurations $|H \rightarrow L+2\rangle$ and $|H \rightarrow L+7\rangle$, for the calculations performed using 6-31G++ and aug-cc-PVTZ type basis sets. But, for the calculations performed with smaller basis sets, the dominant configurations is $|H \rightarrow L+1\rangle$, while the next important configuration can be $|H \rightarrow L+6\rangle$ or $|H \rightarrow L+1; H \rightarrow L+5\rangle$, depending on the basis set. Thus, we can draw the following general conclusion regarding this: (a) for large basis set calculations, for a given peak, the configurations are in perfect agreement with each other, and (b) the

configurations predicted by calculations performed using smaller basis sets such as cc-PVDZ are found to be different as compared to those obtained in larger basis set calculations.

The dominant configurations for the wave functions corresponding to peak I and the most intense peak (peak III) of Li_3 chain, computed using various basis sets are presented in Table S11. We find that for the first peak the dominant configuration is $|H - 1 \rightarrow H\rangle$ for all the basis sets except for aug-cc-pVTZ. For the aug-cc-pVTZ the dominant configurations contributing to the excited state wave function are different compared to other basis sets, because of the reversal of ground and excited states. However, because the peak energies and oscillator strength for the state are in excellent agreement with all other basis sets implies that we have obtained correct quantitative description of the excited states even with this basis set. For peak III the main contribution to the excited state wave function is from $|H - 1 \rightarrow L + 2\rangle$ for the larger 6-311++ and aug-cc class of basis sets, while it is from $|H - 1 \rightarrow L + 1\rangle$ for the smaller cc-pVTZ and cc-pVDZ basis sets.

The main configurations contributing to the excited states wave functions of peak I and the most intense peak (peak IV) of Li_3 triangular cluster, computed using various basis sets are presented in Table S12. We note that for the first peak, the main contribution to the wave function is from configurations $|H \rightarrow L + 14\rangle$ or $|H \rightarrow L + 13\rangle$ for the larger 6-311++G and aug-cc class of basis sets. For the correlation-consistent basis sets (cc-pVDZ and cc-pVTZ) the main contribution is due to the configuration $|H \rightarrow L + 2\rangle$. For the fourth peak, the dominant configuration is $|H - 1 \rightarrow L\rangle$, irrespective of the type of basis set used for the calculation.

The dominant configurations corresponding to the excited states wave functions of peak I and the most intense peak of the spectra (peak II) of the Li_4 cluster are presented in Table S13. For the first peak, the main contribution is from the configuration $|H \rightarrow L + 1\rangle$ for all the basis sets, while for peak II it is $|H - 1 \rightarrow L\rangle$ for all the basis sets. Thus, we have excellent agreement among all the basis sets when it comes to the most important configuration for both the peaks of the Li_4 cluster.

The important configurations corresponding to the excited states wave function of peak I and the most intense peak (peak V) of the photoabsorption spectra of Be_2^+ cluster are presented in Table S14. The dominant configuration contributing to peak I is $|H \rightarrow L\rangle$ for the 6-311++G class of basis sets, and $|H \rightarrow L + 2\rangle$ for the rest. For peak V, the main configuration contributing to the CI wave function is $|H - 1 \rightarrow L + 1\rangle$ for 6-311++G class of basis sets, and $|H - 1 \rightarrow L\rangle$ for the rest of the sets.

The configurations dominating the excited state CI wave functions of peak I and the most intense peak (peak VII) of Be_3^+ cluster are listed in Table S15. We note that the most important configurations contributing to peak I can be classified in two groups: (a) for larger 6-311++G(3df,3pd) and aug-cc class of basis sets the dominant configuration is $|H \rightarrow L + 1\rangle$, (b) while for smaller basis sets dominant configuration is highly basis set dependent. For peak VII, the doubly-excited configurations $|H - 2 \rightarrow L; H \rightarrow L + 2\rangle$ and $|H - 1 \rightarrow L; H \rightarrow L + 4\rangle$ dominate the excited-state wave functions for the larger 6-311++G(3df,3pd) and aug-cc class of basis sets, but vary significantly for the rest.

Most important configurations contributing to the wave functions for peak I and the most intense peak (peak IV) of B_2^+ cluster are presented in Table S16. It is obvious that the double-excitation $|H - 1 \rightarrow L; H \rightarrow L\rangle$ contributes the most to peak I for all the basis sets. The dominant configurations contributing to the wave functions of peak IV are $|H \rightarrow L + 5\rangle$ and $|H \rightarrow L + 11\rangle$ for all the basis sets except the cc-pVDZ/cc-pVTZ, for which instead of $|H \rightarrow L + 11\rangle$, the double excitation $|H - 1 \rightarrow L; H \rightarrow L\rangle$ contributes.

Finally, we present the dominant configurations in the CI wave functions corresponding to peak I, and the most intense peak (peak VIII), of B_3^+ cluster in Table S17. The configuration with maximum contribution to the excited state wave functions for peak I is $|H \rightarrow L\rangle$, irrespective of the basis set. The next dominant configuration is basis-set dependent, however, it is a double excitation in all the cases. The dominant configuration corresponding to the CI wave function of peak VIII is the double excitation $|H - 1 \rightarrow L; H \rightarrow L + 3\rangle$ for all the basis sets.

The detailed wave function analysis for all the peaks of the optical absorption spectra of clusters considered in this work using the largest aug-cc-pVTZ basis set is provided in Table S18-S25 of the SI.

Conclusion

In this work, we presented electron-correlated calculations of the optical absorption spectra of small neutral and ionic clusters using various basis sets. First, the stable geometries of various clusters were determined at the CCSD level of theory, using the aug-cc-pVTZ basis set. For the ground and the excited state wave functions calculations needed to compute the absorption spectra, we used the FCI, QCI, and MRSDCI approaches depending upon the size of the clusters. The CI calculations were performed using six different basis sets, namely, 6-311++G(2d,2p), 6-311++G(3df,3pd), cc-pVDZ, cc-pVTZ, aug-cc-pVDZ, and aug-cc-pVTZ.

We observed that the optical absorption spectra of all these clusters exhibit excellent convergence for all the basis sets in the lower energy range. However, usually after the first two peaks, the shift in peak locations for cc-pVDZ and cc-pVTZ basis set are noted in all likelihood because of the lack of diffuse basis functions in these sets. If we use augmented basis sets, the absorption spectra show good agreement with the results computed using other similar basis sets. Although aug-cc-pVDZ basis set has a relatively smaller number of basis functions as compared to aug-cc-pVTZ basis set, the agreement between the spectra computed using the two basis sets is very good. Because the number of two-electron integrals increases as N^4 where N is the number of basis functions in basis set, we can reduce the computational cost significantly by using aug-cc-pVDZ basis set instead of larger Pople's basis sets, and aug-cc-pVTZ basis set. Thus, our general recommendation is that for optical absorption calculations one should use a basis set containing diffuse functions, i.e., of the aug-cc- type. However, whether one should use aug-cc-pVDZ, or a larger set, should be

decided by the available computational resources.

We believe that the CI calculations presented in this work are quite accurate, as is obvious from the fact that our obtained results are in very good agreement with the experiments for Li_3 and Li_4 clusters. Therefore, it will be of interest to compare our results on other clusters also with the experiments, as and when they are performed.

Associated Content

Supporting Information

In the supporting information file, we have provided the peak locations, oscillator strengths, and dominant excited state configurations corresponding to the optical absorption spectra of all the clusters for all the basis sets considered in this work. The SI file also contains the details of the many-particle wave functions of excited states contributing to the peaks in the optical absorption spectrum of clusters for aug-cc-pVTZ basis set.

Author Information

Corresponding Author

Alok Shukla: Department of Physics, Indian Institute of Technology Bombay, Powai, Mumbai 400076, India; *E-mail: shukla@phy.iitb.ac.in

Acknowledgment

This work was supported by senior research fellowship (DST-Inspire) provided by department of science and technology, India.

Authors

Vikram Mahamiya: Department of Physics, Indian Institute of Technology Bombay, Powai, Mumbai 400076, India; E-mail: mahamiyavikram@gmail.com

Pritam Bhattacharyya: Institute for Theoretical Solid State Physics, Leibniz IFW Dresden, Helmholtzstr. 20, 01069 Dresden, Germany; E-mail: pritambhattacharyya01@gmail.com

Notes

The authors declare no competing financial interests.

References

- (1) Boys, S. F. Electronic Wave Functions. I. A General Method of Calculation for the Stationary States of Any Molecular System. *Proceedings of the Royal Society of London Series A* **1950**, *200*, 542–554.
- (2) McMurchie, L. E.; Davidson, E. R. One- and two-electron integrals over cartesian gaussian functions. *Journal of Computational Physics* **1978**, *26*, 218 – 231.
- (3) Davidson, E. R.; Feller, D. Basis set selection for molecular calculations. *Chemical Reviews* **1986**, *86*, 681–696.
- (4) Huzinaga, S. Basis sets for molecular calculations. *Computer Physics Reports* **1985**, *2*, 281 – 339.
- (5) Huzinaga, S. Gaussian-Type Functions for Polyatomic Systems. I. *The Journal of Chemical Physics* **1965**, *42*, 1293–1302.
- (6) Ruedenberg, K.; Raffanetti, R. C.; Bardo, R. D. *Structure and Reactivity, Proceedings of the 1972 Boulder Conference*; Wiley: New York, 1973.
- (7) Bardo, R. D.; Ruedenberg, K. Even-tempered atomic orbitals. VI. Optimal orbital exponents and optimal contractions of Gaussian primitives for hydrogen, carbon, and oxygen in molecules. *The Journal of Chemical Physics* **1974**, *60*, 918–931.
- (8) Huzinaga, S.; Klobukowski, M.; Tatewaki, H. The well-tempered GTF basis sets and their applications in the SCF calculations on N₂, CO, Na₂, and P₂. *Canadian Journal of Chemistry* **1985**, *63*, 1812–1828.
- (9) Tatewaki, H.; Huzinaga, S. A systematic preparation of new contracted Gaussian type orbital set. I. Transition metal atoms from Sc to Zn. *The Journal of Chemical Physics* **1979**, *71*, 4339–4348.

- (10) Tatewaki, H.; Huzinaga, S. A systematic preparation of new contracted Gaussian-type orbital sets. III. Second-row atoms from Li through Ne. *Journal of Computational Chemistry* **1980**, *1*, 205–228.
- (11) Hehre, W. J.; Stewart, R. F.; Pople, J. A. Self-Consistent Molecular-Orbital Methods. I. Use of Gaussian Expansions of Slater-Type Atomic Orbitals. *The Journal of Chemical Physics* **1969**, *51*, 2657–2664.
- (12) Ditchfield, R.; Hehre, W. J.; Pople, J. A. Self-Consistent Molecular-Orbital Methods. IX. An Extended Gaussian-Type Basis for Molecular-Orbital Studies of Organic Molecules. *The Journal of Chemical Physics* **1971**, *54*, 724–728.
- (13) Binkley, J. S.; Pople, J. A.; Hehre, W. J. Self-consistent molecular orbital methods. 21. Small split-valence basis sets for first-row elements. *Journal of the American Chemical Society* **1980**, *102*, 939–947.
- (14) Binkley, J. S.; Pople, J. A. Self-consistent molecular orbital methods. XIX. Split-valence Gaussian-type basis sets for beryllium. *The Journal of Chemical Physics* **1977**, *66*, 879–880.
- (15) Krishnan, R.; Binkley, J. S.; Seeger, R.; Pople, J. A. Self-consistent molecular orbital methods. XX. A basis set for correlated wave functions. *The Journal of Chemical Physics* **1980**, *72*, 650–654.
- (16) Hariharan, P. C.; Pople, J. A. The influence of polarization functions on molecular orbital hydrogenation energies. *Theoretica chimica acta* **1973**, *28*, 213–222.
- (17) Collins, J. B.; von R. Schleyer, P.; Binkley, J. S.; Pople, J. A. Self-consistent molecular orbital methods. XVII. Geometries and binding energies of second-row molecules. A comparison of three basis sets. *The Journal of Chemical Physics* **1976**, *64*, 5142–5151.

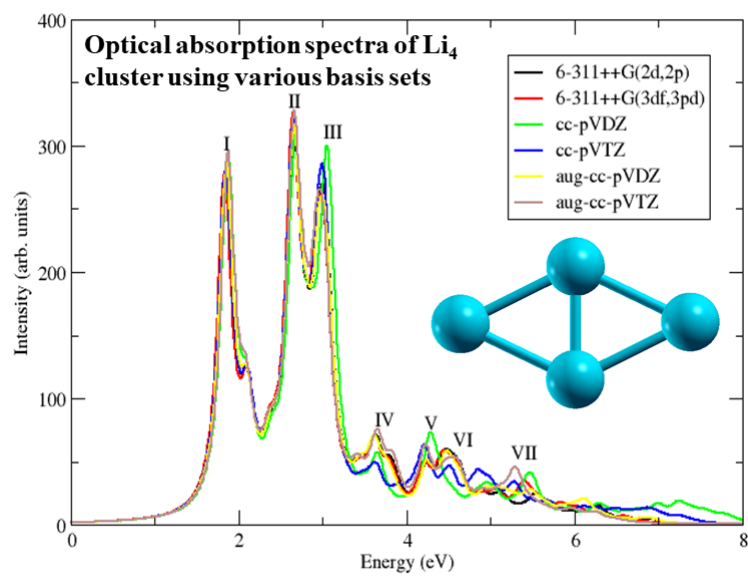
- (18) Francl, M. M.; Pietro, W. J.; Hehre, W. J.; Binkley, J. S.; Gordon, M. S.; DeFrees, D. J.; Pople, J. A. Self-consistent molecular orbital methods. XXIII. A polarization-type basis set for second-row elements. *The Journal of Chemical Physics* **1982**, *77*, 3654–3665.
- (19) Pietro, W. J.; Francl, M. M.; Hehre, W. J.; DeFrees, D. J.; Pople, J. A.; Binkley, J. S. Self-consistent molecular orbital methods. 24. Supplemented small split-valence basis sets for second-row elements. *Journal of the American Chemical Society* **1982**, *104*, 5039–5048.
- (20) Frisch, M. J.; Pople, J. A.; Binkley, J. S. Self-consistent molecular orbital methods 25. Supplementary functions for Gaussian basis sets. *The Journal of Chemical Physics* **1984**, *80*, 3265–3269.
- (21) Dunning, T. H. Gaussian basis sets for use in correlated molecular calculations. I The atoms boron through neon and hydrogen. *The Journal of Chemical Physics* **1989**, *90*, 1007–1023.
- (22) Kendall, R. A.; Dunning, T. H.; Harrison, R. J. Electron affinities of the first-row atoms revisited. Systematic basis sets and wave functions. *The Journal of Chemical Physics* **1992**, *96*, 6796–6806.
- (23) Woon, D. E.; Dunning, T. H. J. The Pronounced Effect of Microsolvation on Diatomic Alkali Halides: Ab Initio Modeling of $\text{MX}(\text{H}_2\text{O})_n$ ($\text{M} = \text{Li}, \text{Na}$; $\text{X} = \text{F}, \text{Cl}$; $n = 1-3$). *Journal of the American Chemical Society* **1995**, *117*, 1090–1097.
- (24) Balakina, M.; Nefediev, S. The choice of basis set for calculations of linear and nonlinear optical properties of conjugated organic molecules in gas and in dielectric medium by the example of p-nitroaniline. *Computational Materials Science* **2007**, *38*, 467–472, Selected papers from the International Conference on Computational Methods in Sciences and Engineering 2004.

- (25) Parsons, T.; Balduf, T.; Cheeseman, J. R.; Caricato, M. Basis Set Dependence of Optical Rotation Calculations with Different Choices of Gauge. *The Journal of Physical Chemistry A* **2022**, *126*, 1861–1870, PMID: 35271772.
- (26) Reis, H.; Papadopoulos, M. G. Nonlinear optical properties of the rhombic B₄-cluster. *Journal of Computational Chemistry* **1999**, *20*, 679–687.
- (27) Lauderdale, W. J.; Coolidge, M. B. Basis set effects on the nonlinear optical properties of selected linear diacetylenes. *The Journal of Physical Chemistry* **1995**, *99*, 9368–9373.
- (28) Jabłoński, M.; Palusiak, M. Basis Set and Method Dependence in Quantum Theory of Atoms in Molecules Calculations for Covalent Bonds. *The Journal of Physical Chemistry A* **2010**, *114*, 12498–12505, PMID: 21049895.
- (29) Frisch, M. J. et al. Gaussian 16 Revision C.01. 2016.
- (30) McMurchie, L. E.; Elbert, S. T.; Langhoff, S. R.; Davidson, E. R. MELD package from Indiana University. It has been modified by us to handle bigger systems.
- (31) Shinde, R.; Shukla, A. Large-scale first principles configuration interaction calculations of optical absorption in aluminum clusters. *Phys. Chem. Chem. Phys.* **2014**, *16*, 20714–20723.
- (32) Rai, D. K.; Chakraborty, H.; Shukla, A. Tunable Optoelectronic Properties of Triply Bonded Carbon Molecules with Linear and Graphyne Substructures. *The Journal of Physical Chemistry C* **2018**, *122*, 1309–1317.
- (33) Chakraborty, H.; Shukla, A. Pariser - Parr - Pople Model Based Investigation of Ground and Low - Lying Excited States of Long Acenes. *The Journal of Physical Chemistry A* **2013**, *117*, 14220–14229.
- (34) Aryanpour, K.; Shukla, A.; Mazumdar, S. Electron correlations and two-photon states

- in polycyclic aromatic hydrocarbon molecules: A peculiar role of geometry. *The Journal of Chemical Physics* **2014**, *140*, 104301.
- (35) Chakraborty, H.; Shukla, A. Theory of triplet optical absorption in oligoacenes: From naphthalene to heptacene. *The Journal of Chemical Physics* **2014**, *141*, 164301.
- (36) SHINDE, R.; SHUKLA, A. LARGE-SCALE FIRST PRINCIPLES CONFIGURATION INTERACTION CALCULATIONS OF OPTICAL ABSORPTION IN BORON CLUSTERS. *Nano LIFE* **2012**, *02*, 1240004.
- (37) Shukla, A. Correlated theory of triplet photoinduced absorption in phenylene-vinylene chains. *Phys. Rev. B* **2002**, *65*, 125204.
- (38) Shukla, A. Theory of nonlinear optical properties of phenyl-substituted polyacetylenes. *Phys. Rev. B* **2004**, *69*, 165218.
- (39) Sony, P.; Shukla, A. Large-scale correlated calculations of linear optical absorption and low-lying excited states of polyacenes: Pariser-Parr-Pople Hamiltonian. *Phys. Rev. B* **2007**, *75*, 155208.
- (40) Basak, T.; Chakraborty, H.; Shukla, A. Theory of linear optical absorption in diamond-shaped graphene quantum dots. *Phys. Rev. B* **2015**, *92*, 205404.
- (41) Priya, P. K.; Rai, D. K.; Shukla, A. Photoabsorption in sodium clusters: first principles configuration interaction calculations. *The European Physical Journal D* **2017**, *71*, 116.
- (42) Shinde, R.; Shukla, A. First principles electron-correlated calculations of optical absorption in magnesium clusters. *The European Physical Journal D* **2017**, *71*, 301.
- (43) Bhattacharyya, P.; Rai, D. K.; Shukla, A. Systematic First-Principles Configuration-Interaction Calculations of Linear Optical Absorption Spectra in Silicon Hydrides: Si₂H_{2n} (n = 1-3). *The Journal of Physical Chemistry A* **2019**, *123*, 8619–8631.

- (44) Wheeler, S. E.; Sattelmeyer, K. W.; Schleyer, P. v. R.; Schaefer, H. F. Binding energies of small lithium clusters (Lin) and hydrogenated lithium clusters (LinH). *The Journal of Chemical Physics* **2004**, *120*, 4683–4689.
- (45) Florez, E.; Fuentealba, P. A theoretical study of alkali metal atomic clusters: From Lin to Csn ($n = 2-8$). *International Journal of Quantum Chemistry* **2009**, *109*, 1080–1093.
- (46) HUBER, K. P. Molecular Structure Constants of Diatomic molecules. *Molecular Spectra and molecular Structure Constants of Diatomic molecules* **1979**,
- (47) Jones, R. O.; Lichtenstein, A. I.; Hutter, J. Density functional study of structure and bonding in lithium clusters Lin and their oxides LinO. *The Journal of Chemical Physics* **1997**, *106*, 4566–4574.
- (48) Srinivas, S.; Jellinek, J. Structural and electronic properties of small beryllium clusters: A theoretical study. *The Journal of Chemical Physics* **2004**, *121*, 7243–7252.
- (49) Hanley, L.; Whitten, J. L.; Anderson, S. L. Collision-induced dissociation and ab initio studies of boron cluster ions: determination of structures and stabilities. *The Journal of Physical Chemistry* **1988**, *92*, 5803–5812.
- (50) Hong, X.; Wang, F. TDDFT calculation for photoabsorption spectra of Lin ($n=2-11,20$) clusters. *Physics Letters A* **2011**, *375*, 1883 – 1888.
- (51) Blanc, J.; Broyer, M.; Chevaleyre, J.; Dugourd, P.; Kühling, H.; Labastie, P.; Ulbricht, M.; Wolf, J. P.; Wöste, L. High resolution spectroscopy of small metal clusters. *Zeitschrift für Physik D Atoms, Molecules and Clusters* **1991**, *19*, 7–12.

For Table of Contents Only



Supporting Information For: Benchmarking Gaussian Basis Sets in Quantum-Chemical Calculations of Photoabsorption Spectra of Light Atomic Clusters

Vikram Mahamiya,^{*,†} Pritam Bhattacharyya,^{*,†,‡} and Alok Shukla^{*,†}

[†]*Department of Physics, Indian Institute of Technology Bombay, Powai, Mumbai 400076, India*

[‡]*Present Address: Institute for Theoretical Solid State Physics, Leibniz IFW Dresden, Helmholtzstr. 20, 01069 Dresden, Germany*

E-mail: mahamiyavikram@gmail.com; pritambhattacharyya01@gmail.com; shukla@phy.iitb.ac.in

Table S1: Comparison of the peak locations of the optical absorption spectra of Li₂ cluster computed using various basis sets.

Basis Set	Peak I (eV)	Peak II (eV)	Peak III (eV)	Peak IV (eV)	Peak V (eV)	Peak VI (eV)	Peak VII (eV)	Peak VIII (eV)	Peak IX (eV)
6-311++G(2d,2p)	1.82	2.61	3.85	4.87	5.88	6.50	7.06	-	-
6-311++G(3df,3pd)	1.83	2.57	3.85	4.61	4.84	5.64	5.88	6.08	7.00
cc-pVDZ	1.82	2.65	4.43	5.95	7.12	-	-	-	-
cc-pVTZ	1.83	2.58	4.26	5.43	5.98	6.64	7.03	-	-
aug-cc-pVDZ	1.82	2.60	3.84	4.58	5.06	5.94	6.67	6.96	-
aug-cc-pVTZ	1.83	2.57	3.87	4.59	5.43	5.93	6.66	7.03	-

Table S2: Comparison of the peak locations of the optical absorption spectra of Li₃ chain computed using various basis sets.

Basis Set	Peak I (eV)	Peak II (eV)	Peak III (eV)	Peak IV (eV)	Peak V (eV)	Peak VI (eV)
6-311++G(2d,2p)	0.72	1.27	2.58	3.39	3.91	4.28
6-311++G(3df,3pd)	0.72	1.27	2.54	3.38	3.90	4.14
cc-pVDZ	0.72	1.26	2.65	3.47	4.37	4.92
cc-pVTZ	0.72	1.28	2.57	3.45	4.39	4.58
aug-cc-pVDZ	0.72	1.26	2.56	3.38	3.88	-
aug-cc-pVTZ	0.72	1.27	2.53	3.37	3.89	-

Table S3: The peak locations of the optical absorption spectra of Li₃ isosceles triangular cluster computed using various basis sets are compared.

Basis Set	Peak I (eV)	Peak II (eV)	Peak III (eV)	Peak IV (eV)	Peak V (eV)	Peak VI (eV)	Peak VII (eV)
6-311++G(2d,2p)	1.09	1.41	2.14	2.41	2.66	2.97	3.21
6-311++G(3df,3pd)	1.07	1.42	2.12	2.39	2.65	2.96	3.19
cc-pVDZ	1.11	1.40	2.18	2.43	2.61	2.81	3.13
cc-pVTZ	1.08	1.42	2.15	2.40	2.70	3.02	4.27
aug-cc-pVDZ	1.09	1.41	2.13	2.40	2.65	2.96	3.20
aug-cc-pVTZ	1.07	1.42	2.11	2.43	2.65	2.95	3.20

Table S4: High energy peak locations of the optical absorption spectra of Li₃ Isosceles triangular cluster computed using various basis sets are compared.

Li ₃ Cluster Basis Set	Peak VIII (eV)	Peak IX (eV)	Peak X (eV)	Peak XI (eV)	Peak XII (eV)
6-311++G(2d,2p)	3.77	4.25	5.29	5.99	-
6-311++G(3df,3pd)	3.75	4.17	4.91	5.25	5.79
cc-pVDZ	3.57	4.24	4.94	5.33	6.05
cc-pVTZ	4.69	5.64	-	-	-
aug-cc-pVDZ	4.16	4.44	5.35	5.59	5.94
aug-cc-pVTZ	3.77	4.11	5.39	5.60	-

Table S5: The peak locations of the optical absorption spectra of Li_4 rhombus cluster computed using various basis sets. The higher energy peak locations are presented in the Table I of the Supporting Information.

Basis Set	Peak I (eV)	Peak II (eV)	Peak III (eV)	Peak IV (eV)	Peak V (eV)	Peak VI (eV)	Peak VII (eV)
6-311++G(2d,2p)	1.84	2.65	3.05	3.64	4.24	4.52	5.15
6-311++G(3df,3pd)	1.83	2.64	2.93	3.63	4.21	4.51	5.11
cc-pVDZ	1.87	2.67	3.08	3.65	4.27	4.86	5.42
cc-pVTZ	1.84	2.65	3.03	3.64	4.22	4.54	5.30
aug-cc-pVDZ	1.85	2.65	3.05	3.61	4.23	4.62	-
aug-cc-pVTZ	1.87	2.65	2.93	3.66	4.22	4.61	5.30

Table S6: The peak locations of the optical absorption spectra of Be_2^+ cluster computed using various basis sets are compared.

Basis Set	Peak I (eV)	Peak II (eV)	Peak III (eV)	Peak IV (eV)	Peak V (eV)	Peak VI (eV)	Peak VII (eV)	Peak VIII (eV)	Peak IX (eV)
6-311++G(2d,2p)	1.75	3.66	4.18	6.04	6.32	8.32	8.90	9.33	9.65
6-311++G(3df,3pd)	1.74	3.68	4.18	6.04	6.30	8.33	8.84	9.31	9.63
cc-pVDZ	1.76	3.69	4.20	6.12	6.37	8.28	9.61	-	-
cc-pVTZ	1.74	3.68	4.19	6.05	6.31	8.44	9.50	-	-
aug-cc-pVDZ	1.77	3.69	4.18	6.08	6.36	8.38	9.09	9.47	-
aug-cc-pVTZ	1.74	3.68	4.18	6.03	6.30	8.34	8.92	9.38	-

Table S7: The peak locations of the optical absorption spectra of Be_3^+ cluster computed using various basis sets are compared.

Basis Set	Peak I (eV)	Peak II (eV)	Peak III (eV)	Peak IV (eV)	Peak V (eV)	Peak VI (eV)	Peak VII (eV)
6-311++G(2d,2p)	1.05	3.16	3.66	4.90	5.39	5.86	6.53
6-311++G(3df,3pd)	1.02	3.17	3.63	4.84	5.40	5.83	6.47
cc-pVDZ	1.04	3.16	3.67	4.91	5.39	5.89	6.52
cc-pVTZ	1.01	3.14	3.60	4.87	5.37	5.83	6.50
aug-cc-pVDZ	1.02	3.16	3.66	4.87	5.41	5.87	6.51
aug-cc-pVTZ	1.02	3.16	3.66	4.87	5.40	5.85	6.52

Table S8: The peak locations of the optical absorption spectra of B_2^+ cluster computed using various basis sets are compared.

Basis Set	Peak I (eV)	Peak II (eV)	Peak III (eV)	Peak IV (eV)	Peak V (eV)	Peak VI (eV)	Peak VII (eV)	Peak VIII (eV)	Peak IX (eV)
6-311++G(2d,2p)	3.65	4.86	6.01	7.00	7.63	9.68	10.26	11.42	12.71
6-311++G(3df,3pd)	3.65	4.77	5.98	7.14	7.62	9.65	10.22	11.40	12.61
cc-pVDZ	3.64	4.79	6.03	7.16	-	9.88	11.29	12.74	
cc-pVTZ	3.66	4.80	5.99	7.05	7.63	9.87	11.12	12.77	-
aug-cc-pVDZ	3.63	4.78	5.98	7.03	7.60	9.66	10.27	11.31	12.52
aug-cc-pVTZ	3.66	4.80	5.99	7.04	7.65	9.65	10.21	11.41	12.20

Table S9: The peak locations of the optical absorption spectra of B_3^+ cluster computed using various basis sets are compared.

B_3^+ Cluster Basis Set	Peak I (eV)	Peak II (eV)	Peak III (eV)	Peak IV (eV)	Peak V (eV)	Peak VI (eV)	Peak VII (eV)	Peak VIII (eV)
6-311++G(2d,2p)	0.82	3.24	5.00	5.38	6.02	7.12	8.09	8.85
6-311++G(3df,3pd)	0.83	3.21	4.99	5.44	6.06	7.17	8.07	8.87
cc-pVDZ	0.96	3.28	5.17	5.59	6.11	7.39	8.21	8.95
cc-pVTZ	0.82	3.23	4.98	5.35	6.03	7.01	8.06	8.79
aug-cc-pVDZ	0.84	3.22	5.00	5.41	6.02	7.10	8.03	8.80
aug-cc-pVTZ	0.84	3.22	5.01	5.45	6.03	7.16	8.08	8.85

Table S10: The peak locations of the optical absorption spectra of B_3^+ cluster employing TD-DFT method with B3LYP functional and computed using various basis sets are compared.

B_3^+ Cluster Basis Set	Peak I (eV)	Peak II (eV)	Peak III (eV)	Peak IV (eV)
6-311++G(2d,2p)	0.94	2.95	5.70	9.35
6-311++G(3df,3pd)	0.95	2.94	5.70	9.35
cc-pVDZ	0.96	3.00	5.73	9.52
cc-pVTZ	0.96	2.95	5.70	9.40
aug-cc-pVDZ	0.96	2.99	5.73	9.40
aug-cc-pVTZ	0.95	2.94	5.70	9.36

Table S11: Comparison of oscillator strengths and the dominant configurations contributing to the many-particle wave functions for peaks I and the maximum intensity peak (peak III) of Li₃ chain calculated using different basis sets. In the “Polarization” column, \parallel indicates photon polarization along the direction of the molecule (longitudinal polarization), while \perp indicates polarization perpendicular to the molecular axis (transverse polarization). ‘H’ and ‘L’ stand for HOMO and LUMO orbitals.

Basis Set	Peak I			Peak III		
	Polarization	f	Wave-function	Polarization	f	Wave-function
6-311++G(2d,2p)	\parallel	0.106	$ H-1 \rightarrow H\rangle$ $ H \rightarrow L+6\rangle$	\perp	0.591	$ H-1 \rightarrow L+2\rangle$
6-311++G(3df,3pd)	\parallel	0.106	$ H-1 \rightarrow H\rangle$ $ H \rightarrow L+5\rangle$	\perp	0.595	$ H-1 \rightarrow L+2\rangle$ $ H \rightarrow L+11\rangle$
cc-PVDZ	\parallel	0.097	$ H-1 \rightarrow H\rangle$ $ H \rightarrow L\rangle$	\perp	0.631	$ H-1 \rightarrow L+1\rangle$ $ H \rightarrow L+3\rangle$
cc-pVTZ	\parallel	0.105	$ H-1 \rightarrow H\rangle$ $ H \rightarrow L\rangle$	\perp	0.618	$ H-1 \rightarrow L+1\rangle$ $ H \rightarrow L+3\rangle$
aug-cc-pVDZ	\parallel	0.101	$ H-1 \rightarrow H\rangle$ $ H \rightarrow L+7\rangle$	\perp	0.603	$ H-1 \rightarrow L+2\rangle$ $ H \rightarrow L+10\rangle$
aug-cc-pVTZ	\parallel	0.106	$ HF\rangle$ $ H-1 \rightarrow H;$ $H-1 \rightarrow L+5\rangle$	\perp	0.594	$ H-1 \rightarrow L+2\rangle$ $ H-1 \rightarrow H;$ $H-1 \rightarrow L+11\rangle$

Table S12: Comparison of oscillator strengths and the dominant configurations contributing to the many-particle wave functions for peaks I and the maximum intensity peak (peak IV) of Li₃ triangular calculated using different basis sets. The rest of the information is same as in the caption of Table S11.

Basis Set	Peak I			Peak IV		
	Polarization	f	Wave-function	Polarization	f	Wave-function
6-311++G(2d,2p)	\parallel	0.127	$ H \rightarrow L+14\rangle$ $ H \rightarrow L+1\rangle$	\parallel	0.465	$ H-1 \rightarrow L\rangle$ $ H \rightarrow L+9\rangle$
6-311++G(3df,3pd)	\parallel	0.131	$ H \rightarrow L+14\rangle$ $ H \rightarrow L+1\rangle$	\parallel	0.459	$ H-1 \rightarrow L\rangle$ $ H \rightarrow L+5\rangle$
cc-PVDZ	\parallel	0.121	$ H \rightarrow L+2\rangle$ $ H-1 \rightarrow L+2\rangle$	\parallel	0.488	$ H-1 \rightarrow L\rangle$ $ H \rightarrow L+4\rangle$
cc-pVTZ	\parallel	0.129	$ H \rightarrow L+2\rangle$ $ H-1 \rightarrow L+2\rangle$	\parallel	0.478	$ H-1 \rightarrow L\rangle$ $ H \rightarrow L+4\rangle$
aug-cc-pVDZ	\parallel	0.126	$ H \rightarrow L+14\rangle$ $ H \rightarrow L+10\rangle$	\parallel	0.469	$ H-1 \rightarrow L\rangle$ $ H \rightarrow L+16\rangle$
aug-cc-pVTZ	\parallel	0.129	$ H \rightarrow L+13\rangle$ $ H \rightarrow L+1\rangle$	\parallel	0.462	$ H-1 \rightarrow L\rangle$ $ H \rightarrow L+5\rangle$

Table S13: Comparison of oscillator strengths and the dominant configurations contributing to the many-particle wave functions for peaks I and the maximum intensity peak (peak II) of Li_4 cluster calculated using different basis sets. The rest of the information is same as in the caption of Table S11.

Basis Set	Peak I			Peak II		
	Polarization	f	Wave-function	Polarization	f	Wave-function
6-311++G(2d,2p)	\parallel	0.628	$ H \rightarrow L + 1\rangle$ $ H \rightarrow L + 8\rangle$	\parallel	0.648	$ H - 1 \rightarrow L\rangle$ $ H - 1 \rightarrow L + 5\rangle$
6-311++G(3df,3pd)	\parallel	0.615	$ H \rightarrow L + 1\rangle$ $ H \rightarrow L + 9\rangle$	\parallel	0.683	$ H - 1 \rightarrow L\rangle$ $ H - 1 \rightarrow L + 6\rangle$
cc-PVDZ	\parallel	0.659	$ H \rightarrow L + 1\rangle$ $ H \rightarrow L + 4\rangle$	\parallel	0.649	$ H - 1 \rightarrow L\rangle$ $ H \rightarrow L + 3\rangle$
cc-pVTZ	\parallel	0.624	$ H \rightarrow L + 1\rangle$ $ H \rightarrow L + 5\rangle$	\parallel	0.678	$ H - 1 \rightarrow L\rangle$ $ H \rightarrow L + 4\rangle$
aug-cc-pVDZ	\parallel	0.634	$ H \rightarrow L + 1\rangle$ $ H \rightarrow L + 9\rangle$	\parallel	0.654	$ H - 1 \rightarrow L\rangle$ $ H - 1 \rightarrow L + 5\rangle$
aug-cc-pVTZ	\parallel	0.656	$ H \rightarrow L + 1\rangle$ $ H \rightarrow L + 9\rangle$	\parallel	0.660	$ H - 1 \rightarrow L\rangle$ $ H - 1 \rightarrow L + 5\rangle$

Table S14: Comparison of oscillator strengths and the dominant configurations contributing to the many-particle wave functions for peaks I and the maximum intensity peak (peak V) of Be_2^+ cluster calculated using different basis sets. The rest of the information is same as in the caption of Table S11

Basis Set	Peak I			Peak V		
	Polarization	f	Wave-function	Polarization	f	Wave-function
6-311++G(2d,2p)	\parallel	0.113	$ H \rightarrow L\rangle$ $ H - 1 \rightarrow H\rangle$	\perp	0.745	$ H - 1 \rightarrow L + 1\rangle$ $ H - 1 \rightarrow L; H \rightarrow L + 2\rangle$
6-311++G(3df,3pd)	\parallel	0.119	$ H \rightarrow L\rangle$ $ H - 1 \rightarrow H\rangle$	\perp	0.749	$ H - 1 \rightarrow L + 1\rangle$ $ H - 1 \rightarrow L; H \rightarrow L + 2\rangle$
cc-PVDZ	\parallel	0.114	$ H \rightarrow L + 2\rangle$ $ H \rightarrow L; H - 1 \rightarrow L\rangle$	\perp	0.736	$ H - 1 \rightarrow L\rangle$ $ H - 1 \rightarrow L + 2; H \rightarrow L + 3\rangle$
cc-pVTZ	\parallel	0.120	$ H \rightarrow L + 2\rangle$ $ H \rightarrow L; H - 1 \rightarrow L\rangle$	\perp	0.749	$ H - 1 \rightarrow L\rangle$ $ H - 1 \rightarrow L + 2; H \rightarrow L + 3\rangle$
aug-cc-pVDZ	\parallel	0.114	$ H \rightarrow L + 2\rangle$ $ H \rightarrow L; H - 1 \rightarrow L\rangle$	\perp	0.768	$ H - 1 \rightarrow L\rangle$ $ H - 1 \rightarrow L + 2; H \rightarrow L + 3\rangle$
aug-cc-pVTZ	\parallel	0.120	$ H \rightarrow L + 2\rangle$ $ H \rightarrow L; H - 1 \rightarrow L\rangle$	\perp	0.757	$ H - 1 \rightarrow L\rangle$ $ H - 1 \rightarrow L + 2; H \rightarrow L + 3\rangle$

Table S15: Comparison of oscillator strengths and the dominant configurations contributing to the many-particle wave functions for peaks I and the maximum intensity peak (peak VII) of Be_3^+ cluster calculated using different basis sets. The rest of the information is same as in the caption of Table S11

Basis Set	Peak I			Peak VII		
	Polarization	f	Wave-function	Polarization	f	Wave-function
6-311++G(2d,2p)	\parallel	0.172	$ HF\rangle$ $ H \rightarrow L\rangle$	\perp	0.655	$ H - 2 \rightarrow L + 1\rangle$ $ H - 1 \rightarrow L + 2\rangle$
6-311++G(3df,3pd)	\parallel	0.184	$ H \rightarrow L + 1\rangle$ $ H - 1 \rightarrow L; H \rightarrow L\rangle$	\perp	0.647	$ H - 2 \rightarrow L; H \rightarrow L + 2\rangle$ $ H - 1 \rightarrow L; H \rightarrow L + 4\rangle$
cc-PVDZ	\parallel	0.178	$ H \rightarrow L\rangle$ $ H - 1 \rightarrow H\rangle$	\perp	0.640	$ H - 2 \rightarrow L + 1\rangle$ $ H - 1 \rightarrow L + 2\rangle$
cc-pVTZ	\parallel	0.169	$ HF\rangle$ $ H - 1 \rightarrow L; H \rightarrow L\rangle$	\perp	0.635	$ H - 2 \rightarrow L; H \rightarrow L + 1\rangle$ $ H - 1 \rightarrow L; H \rightarrow L + 2\rangle$
aug-cc-pVDZ	\parallel	0.180	$ H \rightarrow L + 1\rangle$ $ H - 1 \rightarrow L; H \rightarrow L\rangle$	\perp	0.646	$ H - 2 \rightarrow L; H \rightarrow L + 2\rangle$ $ H - 1 \rightarrow L; H \rightarrow L + 4\rangle$
aug-cc-pVTZ	\parallel	0.179	$ H \rightarrow L + 1\rangle$ $ H - 1 \rightarrow L; H \rightarrow L\rangle$	\perp	0.657	$ H - 2 \rightarrow L; H \rightarrow L + 2\rangle$ $ H - 1 \rightarrow L; H \rightarrow L + 4\rangle$

Table S16: Comparison of oscillator strengths and the dominant configurations contributing to the many-particle wave functions for peaks I and the maximum intensity peak (peak IV) of B_2^+ cluster calculated using different basis sets. The rest of the information is same as in the caption of Table S11

Basis Set	Peak I			Peak IV		
	Polarization	f	Wave-function	Polarization	f	Wave-function
6-311++G(2d,2p)	\parallel	0.026	$ H - 1 \rightarrow L; H \rightarrow L\rangle$ $ H \rightarrow L + 11\rangle$	\parallel	0.910	$ H \rightarrow L + 5\rangle$ $ H \rightarrow L + 11\rangle$
6-311++G(3df,3pd)	\parallel	0.025	$ H - 1 \rightarrow L; H \rightarrow L\rangle$ $ H \rightarrow L + 11\rangle$	\parallel	0.915	$ H \rightarrow L + 5\rangle$ $ H \rightarrow L + 11\rangle$
cc-PVDZ	\parallel	0.025	$ H - 1 \rightarrow L; H \rightarrow L\rangle$ $ H \rightarrow L + 5\rangle$	\parallel	0.965	$ H \rightarrow L + 5\rangle$ $ H - 1 \rightarrow L; H \rightarrow L\rangle$
cc-pVTZ	\parallel	0.024	$ H - 1 \rightarrow L; H \rightarrow L\rangle$ $ H \rightarrow L + 5\rangle$	\parallel	0.942	$ H \rightarrow L + 5\rangle$ $ H - 1 \rightarrow L; H \rightarrow L\rangle$
aug-cc-pVDZ	\parallel	0.028	$ H - 1 \rightarrow L; H \rightarrow L\rangle$ $ H \rightarrow L + 11\rangle$	\parallel	0.895	$ H \rightarrow L + 11\rangle$ $ H \rightarrow L + 5\rangle$
aug-cc-pVTZ	\parallel	0.026	$ H - 1 \rightarrow L; H \rightarrow L\rangle$ $ H \rightarrow L + 11\rangle$	\parallel	0.918	$ H \rightarrow L + 11\rangle$ $ H \rightarrow L + 5\rangle$

Table S17: Comparison of oscillator strengths and the dominant configurations contributing to the many-particle wave functions for peaks I and the maximum intensity peak (peak VIII) of B_3^+ cluster calculated using different basis sets. The rest of the information is same as in the caption of Table S11

Basis Set	Peak I			Peak VIII		
	Polarization	f	Wave-function	Polarization	f	Wave-function
6-311++G(2d,2p)	\perp	0.005	$ H \rightarrow L\rangle$ $ H - 2 \rightarrow L; H \rightarrow L + 1\rangle$	\parallel	0.508	$ H - 1 \rightarrow L; H \rightarrow L + 3\rangle$ $ H - 1 \rightarrow L; H \rightarrow L + 2\rangle$
6-311++G(3df,3pd)	\perp	0.005	$ H \rightarrow L\rangle$ $ H - 1 \rightarrow L; H \rightarrow L + 1\rangle$	\parallel	0.514	$ H - 1 \rightarrow L; H \rightarrow L + 3\rangle$ $ H - 1 \rightarrow L; H \rightarrow L + 2\rangle$
cc-PVDZ	\perp	0.007	$ H \rightarrow L\rangle$ $ H - 1 \rightarrow L; H \rightarrow L + 1\rangle$	\parallel	0.480	$ H - 1 \rightarrow L; H \rightarrow L + 3\rangle$ $ H - 1 \rightarrow L; H \rightarrow L + 3\rangle$
cc-pVTZ	\perp	0.005	$ H \rightarrow L\rangle$ $ H - 1 \rightarrow L; H \rightarrow L + 1\rangle$	\parallel	0.491	$ H - 1 \rightarrow L; H \rightarrow L + 3\rangle$ $ H - 1 \rightarrow L; H \rightarrow L + 2\rangle$
aug-cc-pVDZ	\perp	0.005	$ H \rightarrow L\rangle$ $ H - 1 \rightarrow L; H \rightarrow L + 2\rangle$	\parallel	0.467	$ H - 1 \rightarrow L; H \rightarrow L + 3\rangle$ $ H - 1 \rightarrow L; H \rightarrow L + 3\rangle$
aug-cc-pVTZ	\perp	0.006	$ H \rightarrow L\rangle$ $ H - 1 \rightarrow L; H \rightarrow L + 2\rangle$	\parallel	0.519	$ H - 1 \rightarrow L; H \rightarrow L + 3\rangle$ $ H - 1 \rightarrow L; H \rightarrow L + 3\rangle$

Table S18: Many-particle wave functions of excited states contributing to the peaks in the optical absorption spectrum of Li_2 cluster for aug-cc-pVTZ basis set. 'E' corresponds to excitation energy (in eV) of an excited state, f denotes the oscillator strength for a particular electric dipole transition. In the "[TDM]" column, we present the magnitudes of the transition dipole moments (TDMs) to understand the extent of coupling between the relevant excited state and the ground state. \parallel indicates photon polarization along the direction of the molecule (longitudinal polarization), while \perp indicates polarization perpendicular to the molecular axis (transverse polarization). 'H' and 'L' stand for HOMO and LUMO orbitals. In the "Wave function" column, each number inside the parentheses denotes the coefficient of the corresponding configuration in the CI wave function. GS indicates the ground states wave function of the cluster.

Peak	E (eV)	f	TDM	Polarization	Wave function
GS					$ HF\rangle(0.9520)$ $ H \rightarrow L + 7; H \rightarrow L + 15\rangle(0.0879)$
I	1.83	0.454	3.184	\parallel	$ H \rightarrow L\rangle(0.7523)$ $ H \rightarrow L + 3\rangle(0.3959)$
II	2.57	0.966	2.770	\perp	$ H \rightarrow L + 2\rangle(0.7046)$ $ H \rightarrow L + 7\rangle(0.5914)$
III	3.87	0.049	0.509	\perp	$ H \rightarrow L + 7\rangle(0.6291)$ $ H \rightarrow L + 2\rangle(0.5439)$
V	5.42	0.024	0.303	\perp	$ H \rightarrow L + 16\rangle(0.8509)$ $ H \rightarrow L + 8; H \rightarrow L + 16\rangle(0.1702)$
VI	5.93	0.026	0.421	\parallel	$ H \rightarrow L + 12\rangle(0.2911)$ $ H \rightarrow L; H \rightarrow L + 8\rangle(0.2523)$

Table S19: Many-particle wave functions of excited states contributing to the peaks in the optical absorption spectrum of Li₃ linear cluster for aug-cc-pVTZ basis set. The rest of the information is same as in the caption of Table S18

Peak	E (eV)	f	TDM	Polarization	Wave function
GS					$ H - 1 \rightarrow H\rangle(0.9246)$ $ H - 1 \rightarrow L + 13\rangle(0.0919)$
I	0.72	0.106	2.453	\parallel	$ HF\rangle(0.8814)$ $ H - 1 \rightarrow H; H - 1 \rightarrow L + 5\rangle(0.1436)$
II	1.27	0.503	4.023	\parallel	$ H - 1 \rightarrow H; H - 1 \rightarrow L\rangle(0.5569)$ $ H - 1 \rightarrow H; H - 1 \rightarrow L + 5\rangle(0.5102)$
III	2.53	0.594	3.096	\perp	$ H - 1 \rightarrow L + 2\rangle(0.6262)$ $ H - 1 \rightarrow H; H - 1 \rightarrow L + 11\rangle(0.3628)$
IV	3.37	0.215	1.141	\perp	$ H - 1 \rightarrow L + 7\rangle(0.4255)$ $ H - 1 \rightarrow L + 14\rangle(0.4237)$
V	3.89	0.011	0.343	\parallel	$ H - 1 \rightarrow L + 8\rangle(0.4214)$ $ H - 1 \rightarrow H; H - 1 \rightarrow L + 13\rangle(0.3520)$

Table S20: Many-particle wave functions of excited states contributing to the peaks in the optical absorption spectrum of Li_3 isosceles triangular cluster for aug-cc-pVTZ basis set. The rest of the information is same as in the caption of TableS18

Peak	E (eV)	f	TDM	Polarization	Wave function
GS					$ HF\rangle(0.9102)$ $ H - 1 \rightarrow H\rangle(0.0933)$
I	1.07	0.129	2.222	\parallel	$ H \rightarrow L + 13\rangle(0.4241)$ $ H \rightarrow L + 1\rangle(0.4114)$
II	1.42	0.020	0.767	\parallel	$ H \rightarrow L + 16\rangle(0.5005)$ $ H - 1 \rightarrow L\rangle(0.4115)$
III	2.11	0.352	2.611	\parallel	$ H - 1 \rightarrow H\rangle(0.5806)$ $ H - 1 \rightarrow L + 15\rangle(0.2483)$
IV	2.43	0.462	2.885	\parallel	$ H - 1 \rightarrow L\rangle(0.5537)$ $ H \rightarrow L + 5\rangle(0.3869)$
V	2.65	0.088	1.163	\perp	$ H \rightarrow L + 2\rangle(0.5541)$ $ H \rightarrow L + 12\rangle(0.3375)$
VI	2.95	0.267	1.922	\perp	$ H - 1 \rightarrow L + 2\rangle(0.4766)$ $ H - 1 \rightarrow L + 12\rangle(0.4269)$
VII	3.20	0.117	1.223	\perp	$ H - 1 \rightarrow L + 2\rangle(0.3983)$ $ H \rightarrow L + 12\rangle(0.3579)$
VIII	3.77	0.016	0.417	\parallel	$ H \rightarrow L + 10\rangle(0.3841)$ $ H \rightarrow L + 19\rangle(0.3349)$
IX	4.11	0.029	0.533	\parallel	$ H - 1 \rightarrow L + 14\rangle(0.4375)$ $ H - 1 \rightarrow L\rangle(0.3910)$
X	5.39	0.004	0.171	\parallel	$ H \rightarrow L + 35\rangle(0.2813)$ $ H \rightarrow L + 37\rangle(0.2744)$

Table S21: Many-particle wave functions of excited states contributing to the peaks in the optical absorption spectrum of Li_4 cluster for aug-cc-pVTZ basis set. The rest of the information is same as in the caption of Table S18

Peak	E (eV)	f	TDM	Polarization	Wave function
GS					$ HF\rangle(0.8913)$ $ (H-1) \rightarrow L; H \rightarrow L+18\rangle(0.0791)$
I	1.87	0.656	3.785	\parallel	$ H \rightarrow L+1\rangle(0.5922)$ $ H \rightarrow L+9\rangle(0.4041)$
II	2.65	0.660	3.188	\parallel	$ H-1 \rightarrow L\rangle(0.6193)$ $ H-1 \rightarrow L+5\rangle(0.2910)$
III	2.93	0.316	2.098	\perp	$ H \rightarrow L+7\rangle(0.4577)$ $ H \rightarrow L+20\rangle(0.4174)$
IV	3.43	0.045	0.736	\perp	$ H-1 \rightarrow L+3\rangle(0.3080)$ $ H \rightarrow L+7\rangle(0.2299)$
V	3.66	0.103	1.070	\parallel	$ H \rightarrow L+6\rangle(0.5653)$ $ H \rightarrow L+18\rangle(0.3856)$
VI	4.22	0.077	0.862	\perp	$ H-1 \rightarrow L+3\rangle(0.2380)$ $ H \rightarrow L+20; H \rightarrow L+21\rangle(0.2227)$
VII	4.61	0.063	0.746	\perp	$ H-1 \rightarrow L+3\rangle(0.4044)$ $ H-1 \rightarrow L+12\rangle(0.4026)$
VIII	5.30	0.012	0.300	\parallel	$ H \rightarrow L+33\rangle(0.3681)$ $ H \rightarrow L; H \rightarrow L+6\rangle(0.2294)$

Table S22: Many-particle wave functions of excited states contributing to the peaks in the optical absorption spectrum of Be_2^+ cluster for aug-cc-pVTZ basis set. The rest of the information is same as in the caption of Table S18

Peak	E (eV)	f	TDM	Polarization	Wave function
GS					$ H \rightarrow L\rangle(0.9351)$ $ H-1 \rightarrow L; H \rightarrow L+2\rangle(0.1684)$
I	1.74	0.120	1.680	\parallel	$ H \rightarrow L+2\rangle(0.8403)$ $ H-1 \rightarrow L; H \rightarrow L\rangle(0.3820)$
II	3.67	0.121	0.821	\perp	$ H \rightarrow L+3\rangle(0.6705)$ $ H \rightarrow L+4\rangle(0.6375)$
III	4.19	0.386	1.940	\parallel	$ H-1 \rightarrow L; H \rightarrow L\rangle(0.7268)$ $ H \rightarrow L+2\rangle(0.3897)$
IV	6.01	0.201	0.827	\perp	$ H-1 \rightarrow L\rangle(0.6418)$ $ H-1 \rightarrow L; H \rightarrow L+1\rangle(0.6116)$
V	6.30	0.757	1.566	\perp	$ H-1 \rightarrow L\rangle(0.8762)$ $ H-1 \rightarrow L+2; H \rightarrow L+3\rangle(0.8573)$

Table S23: Many-particle wave functions of excited states contributing to the peaks in the optical absorption spectrum of Be_3^+ cluster for aug-cc-pVTZ basis set. The rest of the information is same as in the caption of Table S18

Peak	E (eV)	f	TDM	Polarization	Wave function
GS					$ H \rightarrow L\rangle(.8776)$ $ H - 1 \rightarrow L + 1; H \rightarrow L\rangle(.1913)$
I	1.02	0.179	2.678702	\parallel	$ H \rightarrow L + 1\rangle(0.8200)$ $ H - 1 \rightarrow L; H \rightarrow L\rangle(0.3257)$
II	3.16	0.433	2.365586	\parallel	$ H - 1 \rightarrow L; H \rightarrow L\rangle(0.6152)$ $ H - 1 \rightarrow L + 1; H \rightarrow L + 1\rangle(0.4714)$
III	3.66	0.028	0.563211	\perp	$ H - 2 \rightarrow L; H \rightarrow L + 2\rangle(0.5209)$ $ H \rightarrow L + 17\rangle(0.4125)$
IV	4.87	0.020	0.407823	\perp	$ H - 1 \rightarrow L + 1; H \rightarrow L + 2\rangle(0.5211)$ $ H \rightarrow L + 17\rangle(0.3217)$
V	5.40	0.204	1.242734	\parallel	$ H - 2 \rightarrow L; H \rightarrow L + 1\rangle(0.6337)$ $ H - 1 \rightarrow L; H \rightarrow L\rangle(0.3104)$
VI	5.85	0.054	0.612656	\perp	$ H - 1 \rightarrow L; H \rightarrow L + 4\rangle(0.4315)$ $ H - 1 \rightarrow L; H - 1 \rightarrow L + 2; H \rightarrow L\rangle(0.2864)$
VII	6.52	0.657	2.028291	\perp	$ H - 2 \rightarrow L; H \rightarrow L + 2\rangle(0.4960)$ $ H - 1 \rightarrow L; H \rightarrow L + 4\rangle(0.4653)$

Table S24: Many-particle wave functions of excited states contributing to the peaks in the optical absorption spectrum of B_2^+ cluster for aug-cc-pVTZ basis set. The rest of the information is same as in the caption of Table S18

Peak	E (eV)	f	TDM	Polarization	Wave function
GS					$ H \rightarrow L\rangle(.9033)$ $ H - 2 \rightarrow L; H - 1 \rightarrow L + 2\rangle(.1271)$
I	3.66	0.026	0.537	\parallel	$ H - 1 \rightarrow L; H \rightarrow L\rangle(0.7250)$ $ H \rightarrow L + 11\rangle(0.2622)$
II	4.80	0.029	0.496	\parallel	$ H - 1 \rightarrow L + 1; H \rightarrow L + 1\rangle(0.5092)$ $ H - 1 \rightarrow H\rangle(0.4944)$
III	5.99	0.019	0.364	\perp	$ H - 1 \rightarrow L; H \rightarrow L + 2\rangle(0.6138)$ $ H - 2 \rightarrow L\rangle(0.4445)$
IV	7.04	0.918	2.307	\parallel	$ H \rightarrow L + 11\rangle(0.4808)$ $ H \rightarrow L + 5\rangle(0.4713)$
V	7.65	0.009	0.216	\perp	$ H - 2 \rightarrow L\rangle(0.5322)$ $ H - 1 \rightarrow L; H \rightarrow L + 2\rangle(0.4844)$

Table S25: Many-particle wave functions of excited states contributing to the peaks in the optical absorption spectrum of B_3^+ cluster for aug-cc-pVTZ basis set. The rest of the information is same as in the caption of Table S18

Peak	E (eV)	f	TDM	Polarization	Wave function
GS					$ HF\rangle(0.8535)$ $ H - 1 \rightarrow L + 1\rangle(0.1393)$
I	0.84	0.006	0.524	\perp	$ H \rightarrow L\rangle(0.8572)$ $ H - 1 \rightarrow L; H \rightarrow L + 2\rangle(0.1319)$
II	3.22	0.083	0.726	\parallel	$ H - 1 \rightarrow L\rangle(0.8246)$ $ H - 1 \rightarrow L; H - 1 \rightarrow L + 1\rangle(0.1642)$
III	5.01	0.053	0.463	\parallel	$ H - 1 \rightarrow L; H - 1 \rightarrow L\rangle(0.5482)$ $ H \rightarrow L; H \rightarrow L + 1\rangle(0.3184)$
IV	5.45	0.013	0.217	\parallel	$ H \rightarrow L; H \rightarrow L + 1\rangle(0.5721)$ $ H \rightarrow L; H \rightarrow L + 2\rangle(0.5675)$
V	6.03	0.026	0.295	\parallel	$ H \rightarrow L + 3\rangle(0.3937)$ $ H - 1 \rightarrow L + 2\rangle(0.3723)$
VI	7.16	0.026	0.382	\parallel	$ H \rightarrow L + 1; H \rightarrow L + 2\rangle(0.5866)$ $ H \rightarrow L; H \rightarrow L + 1\rangle(0.4308)$
VII	8.08	0.059	0.380	\parallel	$ H - 1 \rightarrow L; H - 1 \rightarrow L + 1\rangle(0.4529)$ $ H - 1 \rightarrow L; H - 1 \rightarrow L + 2\rangle(0.3162)$
VIII	8.85	0.519	1.091	\parallel	$ H \rightarrow L + 3; H - 1 \rightarrow L\rangle(0.3762)$ $ H \rightarrow L + 3; H - 1 \rightarrow L\rangle(0.3748)$

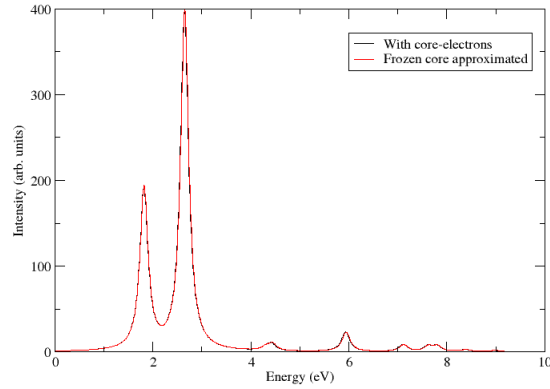


Figure S1: Validation of frozen core approximation for the optical absorption spectra of Li_2 cluster employing QCI method.

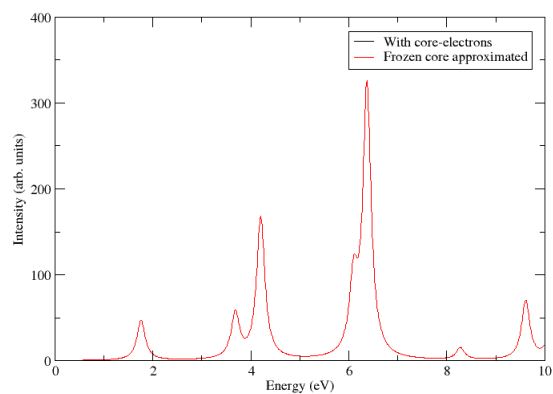


Figure S2: Validation of frozen core approximation for the optical absorption spectra of Be_2^+ cluster employing QCI method.

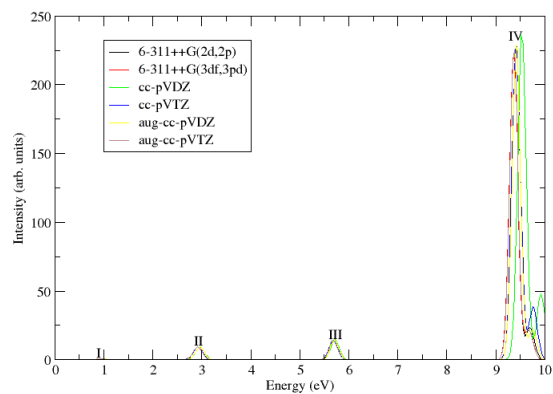


Figure S3: Optical absorption spectra of B_3^+ cluster computed using various basis sets employing B3LYP functional and TD-DFT method.